On the Influence of Uncertainty in Computational Simulations of a High-Speed Jet Flow from an Aircraft Exhaust

Francisco-Javier Granados-Ortiz[a], Carlos Pérez Arroyo[b,c], Guillaume Puigt[c,d], Choi-Hong Lai[a], Christophe Airiau[e]

[a] *University of Greenwich, Old Royal Naval College, Park Row, SE10 9LS, London (UK)*
[b] *University of Sherbrooke, 2500 Boulevard de l'Université, Sherbrooke, QC J1K 2R1, (Canadá)*
[c] *CERFACS, 42 avenue Coriolis, 31057 Toulouse Cedex (France)*
[d] *ONERA/DMPE, Université de Toulouse, F-31055 Toulouse (France)*
[e] *IMFT, Université de Toulouse, UMR 5502 CNRS/INPT-UPS, Allée du professeur Camille Soula, 31400 Toulouse (France)*

Abstract

A classic approach to computational fluid dynamics is to perform simulations with a fixed set of variables in order to account for parameters and boundary conditions. However, experiments and real-life performance are subject to variability in their conditions. In recent years, the interest of performing simulations under uncertainty is increasing, but this is not yet a common rule, and simulations with lack of information are still taking place. This procedure could be missing details such as whether sources of uncertainty affect dramatic parts in the simulation of the flow. One of the reasons of avoiding to quantify uncertainties is that they usually require to run an unaffordable number of CFD simulations to develop the study.

To face this problem, Non-Intrusive Uncertainty Quantification (UQ) has been applied to 3D Reynolds-Averaged Navier-Stokes simulations of an under-expanded jet from an aircraft exhaust with the Spalart-Allmaras turbulent model, in order to assess the impact of inaccuracies and quality in the simulation. To save a large number of computations, sparse grids are used to compute the integrals and built surrogates for UQ. Results show that some regions of the jet plume can be more sensitive than others to variance in both physical and turbulence model parameters. The Spalart-Allmaras turbulent model is demonstrated to have an accurate performance with respect to other turbulent models in RANS, LES and experimental data, and the contribution of a large variance in its parameter is analysed. This investigation explicitly outlines, exhibits and proves the details of the relationship between diverse sources of input uncertainty, the sensitivity of different quantities of interest to said uncertainties and the spatial distribution arising due to their propagation in the simulation of the high-speed jet flow. This analysis represents first numerical study that provides evidence for this heuristic observation.

Keywords: Uncertainty, Sensitivity, CFD, Jets, RANS

1. Introduction

During the last twenty years, accurate industrial simulations were based on the use of Computational Fluid Dynamics (CFD). To this end, a computational domain is first defined around

the object, meshed and then the computation launched once boundary conditions are defined. To compare numerical simulations and experimental data, the choice of boundary conditions is most influential on the results and researchers generally choose the conditions according to data provided by experimentalists. However, this data could be an incomplete input to simulations if not precisely defined by accounting relevant variations. All these factors, in addition to the solver errors (discretisation, numerical schemes, etc.), lead to differences between the 'physical' model and its numerical approximation.

To minimise the discrepancy between the computational and experimental analysis has become important in the recent years, since trends indicate a growing reliance on computational studies as opposed to experimental investigations. A good indicator of this trend is noticed in modern design of aircraft engines, where these designs used to require a 90% of experimental tests and 10% of computational approach, but nowadays the situation has been reversed [61]. Within this context, both accuracy and robustness of the design (low sensitivity to uncertain parameters) are necessary to assess the performance of the CFD representation of the real-world, which is a relevant topic for certification [96]. Improvements in this field could also reduce the certification costs, thanks to the availability of more reliable softwares. One of the key aspects of CFD is that they are, generally, a cheaper option for product design and development than experiments. Actually, CFD simulations are routinely used in fields like optimisation [88, 37], aerospace & aerodynamic industry [55], fire safety modelling [94], heat transfer [65] or nuclear energy [54], amongst many others. Much effort has been spent to develop such techniques, leading to the most reliable simulations for decision-making purposes.

To improve computational simulations, finding a proper way to provide measures of accuracy (as most experimentalists do) is of interest in its own right, since variations in real-life performance must be accounted. This brings in the use to the concept of Uncertainty Quantification (UQ). UQ is about determining *how likely the outputs of a model (numerical or otherwise) are when the inputs are not precisely defined* [77]. Once the input uncertainties are modelled, then it is necessary to find an appropriate UQ methodology. In essence, UQ may be defined as the field of identifying, quantifying and reducing uncertainties and variabilities associated with numerical algorithms, mathematical models, experiments and their predictions of quantities of interest [86]. Regarding the predictions of quantities of interest, one of the central steps in the UQ methodology is determining how likely the outputs of a model are when the inputs undergo variability.

Let us consider a mathematical model symbolically represented by the function $\hat{y}(\xi, x)$, of the random variables $\xi_1, \xi_2, \ldots, \xi_{N_\xi}$, with N_ξ the dimension of the random input space. These variables can represent a large variety of parameters in a problem, such as temperatures, volume flow rate, pressure, etc. When their variation is modelled by probabilistic functions based on their own performance, the objective is to extract information of the imprecision or variation in the output of $\hat{y}(\xi, x)$, say x the spatial coordinate for instance. Another important study that can be extended from UQ is the Sensitivity Analysis. According to [77], this is the study of *how uncertainty in the output of a model can be apportioned to different sources of uncertainty in the*

model input. Ideally, Sensitivity Analysis and UQ should be run one after another, with uncertainty analysis usually preceding sensitivity analysis. This mathematical approach undoubtedly helps to rank the most influential random inputs and provides decision-making solutions. Also, understanding the sensitivity of model output to input parameter uncertainty can be exploited to direct experimental work in order to reduce uncertainty in identified influential parameters, neglecting the non-influential ones [85].

Regarding the sources of uncertainty, these are classified as aleatoric or epistemic. Aleatoric uncertainty is considered as inherent to the variability in a physical quantity. Other terminologies in the literature include irreducible uncertainty, inherent uncertainty, variability and stochastic uncertainty [63]. Another source of inaccuracy is the epistemic uncertainty, which is due to a lack of knowledge. This type of uncertainty could be reduced by the introduction of additional information [75]. Epistemic uncertainty associated with the fidelity of the simulation can have a remarkable impact on the performance. Discrepancies between these simulations and high fidelity data (*e.g.* Large Eddy Simulations or Direct Numerical Simulations) may be substantially due to epistemic uncertainties in the turbulence closures used. For instance, in [14] uncertainty is quantified by using both RANS and LES in a heat transfer problem demonstrating that there is a strong interconnection between uncertainties related to the unknown conditions (aleatoric) and those related to the physical model (epistemic). One can also find applications and definitions for uncertainty in turbulent flows for instance in [58, 59, 53]. In these works, there are two distinctions of the type of uncertainties from the turbulence modelling: in the selection of the turbulence model closure (structural uncertainty) and in the value of the model coefficients (parametric uncertainty). Regarding the turbulence analysis in this paper, a comparison between different turbulent models is developed, but the main objective is focused on the parametric uncertainty that arises in the selection of the appropriate value for the laminar viscosity ratio of the Spalart-Allmaras turbulent model. Another important source of inaccuracy is the numerical error. These can be consequence of the spatial discretisation, temporal discretisation or discrete representation of nonlinear interactions [63]. To measure the spatial discretisation error due to the selection of the mesh is a priority in CFD, and this study is developed in Section 2.2.

First of all, with the available information, a decision has to be made in terms of dealing with uncertainty under either a probabilistic or non-probabilistic framework. In the probabilistic approach, a more detailed (statistical) analysis is developed since the beginning, as the input uncertainty are to be modelled as probabilistic distributions. In addition, not only statistical moments but also output probabilistic distributions of quantities of interest can be computed. As in this manuscript only probabilistic uncertainty is of interest (probabilistic UQ will be referred to as UQ throughout this paper), no more details are given on non-probabilistic approaches, but the reader is suggested to see [86, 100, 23, 73, 108, 19, 48, 101] for further information and applications.

Broadly speaking, there are two ways to implement UQ with a CFD solver. On one hand, the solver can be adapted to deal with uncertain parameters that are related to a predefined probabil-

ity density function. This probability function can be introduced in the original set of equations. With this approach, new equations are then derived, which requires alterations to the computational code of the CFD solver. In the literature, this methodology is known as **intrusive**, and the new set of equations must be changed or adapted depending on the probability functions and on which variables it is applied.

Of course, the introduction of UQ in the solver makes the approach efficient and direct. However, including it in industrial solvers composed of hundred of thousands of lines is cumbersome and may introduce errors to a validated and verified code. Also, if the stochastic output has to be adapted as input to other softwares (*e.g.* to use the CFD mean flow for uncertainty quantification in stability analysis by means of Parabolised Stability Equations [35, 8, 7]) it is not recommendable to code inside all the softwares. Thus, **non-intrusive** UQ is a good alternative as it interacts with the solver being treated as a black-box. In this case, the system of equations that governs the problem is decoupled, and several deterministic computations are run (based on a Design of Experiment which depends on the method) to compute the statistical moments and/or build surrogate models. Non-intrusive and intrusive approaches have been studied in the literature. In [71] Polynomial Chaos (PC) is applied both in an intrusive and non-intrusive way. When the method is coded as an intrusive tool, all dependent variables and random parameters in the Euler equations were replaced with the PC expansions, and applied to three different problems matching very well with the benchmark results. However, experience suggests that for complex problems involving 3D Navier-Stokes computations of turbulent flows on complex surfaces might not be straightforward and it is also time consuming to implement, being non-intrusive a more suitable approach. In [64] intrusive and non-intrusive PC approaches are compared to develop an uncertainty study on an airfoil with randomness in the Mach number and angle of attack. Results obtained are very similar in the comparison, with minor differences.

Once the problem is properly defined, it is required to find the best methodology for uncertainty/sensitivity analysis. Sampling methods are a very reliable non-intrusive technique, since they deal with the solver/model as a black-box, simply requiring many model evaluations to construct the desired output statistical information. Monte-Carlo simulations [56] are a very popular and well established sampling approach. This well known method is generally described by a random sequence of numbers to represent a sample of a population, from which statistical moments of the parameter of interest can be obtained [38]. There is a huge amount of work on the application of the Monte-Carlo technique in many fields. Some examples can be found in [62, 85, 29, 32]. However, in CFD this method has a disadvantage: the large number of model evaluations often required in seeking convergence.
A good approach to deal with the problem of running a CFD simulation for each sample point is to build a surrogate model. This model takes the form

$$y(\boldsymbol{\xi}) = \hat{y}(\boldsymbol{\xi}) + \epsilon(\boldsymbol{\xi}), \tag{1}$$

with y being the exact model, $\hat{y}$ the surrogate model and ϵ the difference between the surrogate and the exact formulation, all defined in $\boldsymbol{\xi}$ space. Several possibilities are available in the literature and there are many examples of the use of surrogate models, such as [97, 83, 30]. Amongst

them, Kriging (also known as Gaussian Process regression) has been preferred in this work because of its robustness, efficiency and simplicity in the implementation. Examples using this method can be Sensitivity Analysis [102], topography [50] or prototyping [40]. Kriging is a frequent approach in CFD. It is actually a well known method in optimisation studies because of its ability to deal with many variables or complex scenarios, as in aircraft wing optimisation involving 45 shape parameters [49], in [11] applied to aerodynamic optimisation of civil structures, and in CFD optimization of aeronautical combustion chambers [25] by means of Kriging predictors combined with the NSGA-II optimisation algorithm [21]. Kriging is not only popular in optimisation, but it is also frequently used in UQ. Successful applications can be found in the literature as follows. In [26] a flexible non-intrusive Kriging approach is developed, aimed to problems with many uncertain parameters and costly evaluations of a model. Gradients from the adjoint of deterministic equations are used on the Kriging surfaces together with sparse grids, to improve the efficacy of the approach. The method is successfully applied to a 2D NACA airfoil problem with a random geometry parametrised by 4 variables. This gradient approach was also presented in [20] related to the perturbation method, applied to the study of interaction of a fluid and a flexible panel. In [47] a Kriging-model-based UQ method is presented for non-smooth responses, which improves other popular approaches in the literature in terms of accuracy and robustness, and it is successfully applied to a transonic RAE 2822 airfoil under normal uncertainty sources. In [51] a UQ study is carried out on 15 normally distributed random variables using Kriging surrogates and an adjoint approach for viscous hypersonic flows.

It is above mentioned that the use of surrogate models is an alternative to direct sampling. However, it is not the only option to overcome the problem. The generalised Polynomial Chaos (gPC) [91, 107] is a spectral method and as such, an important advantage is that one can decompose a random representation into a truncated expansion with deterministic and stochastic components separated. It can be extended to a wider family of basis functions than the original Polynomial Chaos method and it is a very popular approach in the literature with successful applications in many fields. An advantage of this method is that global Sensitivity Analysis can be done without extra costs straightaway from UQ. Thus, in applications with high interest in both UQ and Sensitivity Analysis, it is a very recommended method. The gPC has been successfully applied to several CFD problems in the past and it is a very popular approach to UQ in the literature. Some interesting applications in the literature could be [17], where the effect of inlet uncertainties of swirling flows in pipes is analysed, or [27] where gPC performance is compared to Stochastic Collocation method. In [41] gPC is applied to the stochastic CFD analysis of a pressure probe designed for three-dimensional supersonic flow measurements with moderate swirl, with three uncertain geometrical parameters, and results are successfully compared to Monte-Carlo, with minor differences in the calculated Mach number, which may be product of neglecting viscous effects in CFD simulations or experimental tolerances. In [69] uncertainty in hot gas turbines is analysed. Since one of the most critical parameters in the design process of cooled hot gas components is the Back Flow Margin, gPC is applied to measure the probability of hot gas ingestion and the sensitivity to random parameters, since a deficient design may lead to component failure.

The present paper deals with the analysis on the influence of experimental and parametric uncertainty from the turbulence intensity in the computation of an under-expanded jet flow in the presence of shock-cells. For the Spalart-Allmaras turbulence model, the turbulent intensity is taken into account through the turbulent to laminar viscosity ratio R_t defined for the injection boundary condition. In the literature was pointed out that shock position can be sensitive to input uncertainty as in [105], where transonic airfoils are under study. Actually, from a UQ methodology side, to have shock or series of expansions and compressions can add complexity to the problem. In [82] the existence of a shock made necessary to test large values in the polynomial chaos order expansion and many collocation points, again in a transonic airfoil, and based on Mach number and angle of attack as uncertain. Converged solutions are obtained with few number of collocation points along most of the profile, except in the region of the shock movement for the pressure, and also in the separated area zone for the skin-friction coefficient. All this information is relevant for the application in the present paper. Moreover, in compressible supersonic jet flows, UQ can be specially interesting: the imperfectly expanded conditions generate shock-cells and small changes in input parameters that may lead to relevant variations in shock-cell position and then to noise emission [93, 66, 68]. This effect currently represents a major concern in robust design because of environmental regulations and the challenge of perceived noise reduction of 65% by 2050 with respect to the values dated from the year 2000 [16].

From the turbulence side, uncertainty associated to this modelling has been also matter of study in CFD. In [78], epistemic uncertanty from turbulence modelling for transonic wall-bounded flows is under study in several problems with different eddy-viscosity models. Similarly, in [72] Probabilistic Collocation is employed to quantify uncertainty in CFD RANS simulations of a turbulent flat plate and an airfoil. In [53], polynomial chaos is applied for Sensitivity Analysis in parametric uncertainty in turbulent computations. In that paper it is investigated that different turbulent scales of the LES solution respond differently to the variability in the Smagorinsky constant, and indicates that small scales are mainly affected by changes in the subgrid-model parametric uncertainty.

RANS simulations are still very popular amongst both academic and industrial design processes. However, it is well known that these time-averaged simulations have important deficiencies to simulate turbulent flows, especially for high speed jets. For this reason, specific modified two-equation turbulence models were investigated to improve simulations of turbulent jet flows. A review of these can be found in [46]. Despite these improvements, RANS still lacks robustness and consistency in their jet flow predictions. Factors like jet flow mixing, growth of instabilities or potential core length simulation are challenging in RANS [33], and standard calibrations from other CFD problems do not work often, being necessary to find an appropriate turbulent model parameter setting [22]. All these drawbacks in the prediction, summed to the already mentioned drawbacks inherent to using fixed values for physical conditions, lead to the necessity of providing extra metrics of reliability in the simulations. To this aim, Uncertainty Quantification and Sensitivity Analysis in jet flows can be an interesting application.

There is a dearth of literature about UQ applied to compressible jets. Some examples on the

use of uncertainty in jets will be described in the following. In [2] uncertainty analysis has been applied to CFD simulations of synthetic jets by means of polynomial chaos. In that paper, two cases are analysed: with and without a cross flow under uncertain velocity. In [34] an epistemic uncertainty analysis of an under-expanded jet in a cross flow for turbulent mixing purposes is analysed. In their work, the sources of uncertainty in RANS simulations of turbulent mixing are the Reynolds stresses in the momentum equations and the scalar fluxes in the scalar transport equations. The perturbation of the eigenvalues of the Reynolds stress anisotropy tensor is based in the position in a barycentric triangle map, whose corners represent different limiting states of turbulence anisotropy referred to by their corresponding number of components. This method was also successfully implemented to high speed aircraft nozzle jets in [59], where uncertainty envelopes are obtained for the SST $k-\omega$ turbulent model in four different jet flow problems and compared to Particle Image Velocimetry data. Throughout their paper has been highlighted the importance of providing uncertainty bounds in RANS simulations and the results suggest that the uncertainty analysis can account most of the model inadequacy. This approach introduced in [59, 34, 43] has been often used in the literature by certain authors. In [57] and [3] a similar analysis is carried out on a hypersonic jet flow. In [57], pressure and temperature are varied a ±5%, and Monte Carlo is applied for the measure of aleatoric uncertainty. A study of the epistemic uncertainty is developed as well. Variations on the turbulent kinetic energy and envelopes for the coefficient of friction and pressure are shown. In [60, 43] some tests using enveloping models are presented. These tests include several aerospace designs such as a turbulent flow through an asymmetric diffuser, a turbulent flow over a backward facing step, a subsonic and a supersonic jet flow and two airfoils. These analysis were run in the Stanford University Unstructured (SU2) CFD suite. The supersonic jet corresponds to the axisymmetric convergent-divergent nozzle in [79]. The jet efflux is a Mach 2.0 flow with Reynolds number $Re = 1.3 \times 10^6$. The uncertainty analysis on the Mach and pressure variation along the centreline shows that RANS models over predicts the extent of the jet potential core, but with most experimental data points lying within the computed envelopes. Additionally, in [92], the authors develop a data driven procedure to quantify the structural uncertainty in RANS models when applied to heated supersonic jet flows.

The main objective of the present paper is to develop a study on the influence of both experimental and parametric uncertainty from the turbulence intensity in the computation of an under-expanded jet flow. The one-equation Spalart-Allmaras turbulence model is not popular for this type of jets, so a detailed analysis on its performance is envisaged. Non-Intrusive UQ methods have been applied to 3D steady Reynolds-Averaged Navier-Stokes (RANS) simulations with ***elsA*** solver [13], of which the set-up is described in Section 2. Due to the fact that popular sampling methods such as Monte-Carlo are impractical in terms of computational cost, UQ is deployed with two different approaches. First, generalised Polynomial Chaos [107] is applied to quantify the uncertainty in Section 3. Second, for the purpose of comparison, Kriging surrogates are built to ensure the quality of the analysis. In Section 4, a Sensitivity Analysis is conducted with both methods, in order to assign to each input uncertainty its contribution to the total variance. This work-flow provides a useful framework to assess the influence of relevant parameters in the CFD simulation.

2. CFD simulations

2.1. Simulation set-up

The simulation is based on the cold supersonic under-expanded single jet that was tested experimentally by André [6]. The jet is produced from a convergent nozzle with an exit diameter of $D = 38.0mm$ and a modelled nozzle lip thickness of $t = 0.125D$. The nozzle is operated under-expanded at the stagnation to ambient pressure ratio $NPR = p_s/p_{amb} = 2.27$, with p_s the stagnation pressure and p_{amb} the ambient one. The Reynolds number, Re, based on the jet exit diameter is 1.25×10^6 and the fully expanded jet Mach number is $M_j = 1.15$. The fully expanded Mach number, *i.e.* the Mach number that would be reached if the jet was able to expand further to ambient conditions, is related to the total pressure by

$$NPR = \frac{p_s}{p_{amb}} = \left(1 + \frac{\gamma - 1}{2} M_j^2\right)^{\gamma/(\gamma-1)}. \tag{2}$$

For the boundary conditions used in the computations, the interior/exterior and lip walls of the nozzle are computed with adiabatic no-slip wall conditions. A characteristic approach is chosen to define the inflow conditions outside the nozzle. Such a condition works for all configurations (inflow/outflow, subsonic/supersonic): the number of fields to impose (1, 4 or 5) is chosen according to the local analysis of the waves that travel across the interface. The remaining lateral and outlet boundary conditions are set to a subsonic characteristic ones, where the reference ambient pressure is defined.

The computational domain used for the RANS simulations extends $100D$ in the axial direction and $50D$ in the radial direction. The interior of the nozzle is modeled up to $6D$ while the exterior up to $9D$.

2.2. Mesh generation

The converged 3D mesh consists of a butterfly type mesh to avoid the singularity at the axis as shown in Fig. 1 (b). It contains 20×10^6 cells with roughly $(900 \times 300 \times 64)$ cells in the axial, radial and azimuthal directions respectively forward to the nozzle exit plane, $(220 \times 120 \times 64)$ inside the nozzle and $(170 \times 100 \times 64)$ outside.

The nozzle is wall-resolved for all the conditions with $y^+ \approx 1$ and radially stretched up to the end of the domain at a rate of 10% as can be seen in Fig. 1 (a). Axially, the mesh is uniform at the exit of the nozzle, then it is stretched at 6% up to $0.25D$. Next, it is kept constant up to $10D$, in order to have a minimum of around 40 cells per shock-cell (measured at the last cell, which due to the flow physics, it is the most shortened shock-cell). The mesh is axially stretched again up to the end of the domain at a rate of 10%.

In uncertainty quantification it is necessary to have a converged mesh for all deterministic simulations. This requirement is particularly important for flows containing shocks. In this under-expanded jet, the shock-cells are actually a series of expansion and compression waves that look like widen shocks. The above mentioned mesh has been thoroughly tested and obtained with the following convergence procedure using as reference parameter the Mach number profile at the centreline for the deterministic base case and conditions with a higher NPR. First, the mesh

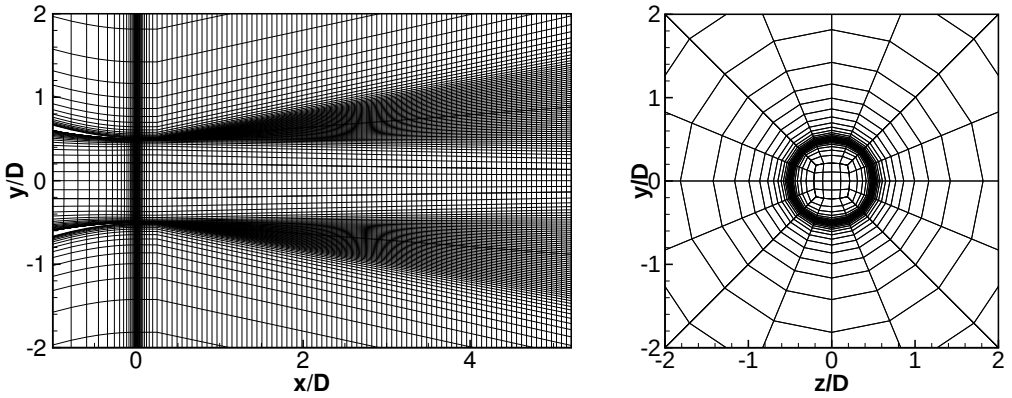

(a) (b)

Figure 1 Mesh cuts representing every fourth cells in the plane **(a)** $z/D = 0$ and the plane **(b)** $x/D = 0$.

has been converged azimuthally with 64 cells, obtaining a relative error with respect to a refined mesh of less than 0.15% as shown in Fig. 2 (a). Second, the axial discretization is taken into account by varying the starting position where the mesh topology is uniform. Axial convergence is obtained with an error of 0.2% with respect to the most refined mesh for the position of $0.25D$ as shown in Fig. 2 (b). Relative errors of the same order of magnitude are obtained for the axial velocity at x/D=1. Finally, the y^+ has been checked so that it still lays in the range smaller than unity for the range of working conditions presented in Section 3.1.

2.3. Numerical formulation

The full three-dimensional compressible Reynolds-Averaged Navier-Stokes equations have been solved by using the Finite Volume multi-block structured solver ***elsA*** (Onera's software [13]) and will be briefly explained here. The turbulence model used in the computations of this work is the one-equation Spalart-Allmaras (S-A) standard model [89]. The convective flux is computed using an upwind approach based on the Roe's approximate Riemann solver [76]. The scheme's accuracy is increased by the use of either a second order MUSCL extrapolation [98] coupled with the minmod limiter or a third order extrapolation technique [15]. The implicit system is solved at $CFL = 100$ with a $LU - SSOR$ algorithm with four sweeps [103]. In order to accelerate the convergence for all the conditions, a converged deterministic base case solution has been used as initial solution. The numerical ingredients considered in this study follow the recommendations regarding the simulations of subsonic jet flows using the RANS modelling shown in [24].

2.4. Turbulence model

In the literature, it is generally admitted that the $k - \omega$ turbulence model gives the best results for jets. However, with respect to other turbulence models, the use of the one-equation turbulence S-A model can be useful and the study of its performance for jet flows can be of interest. By

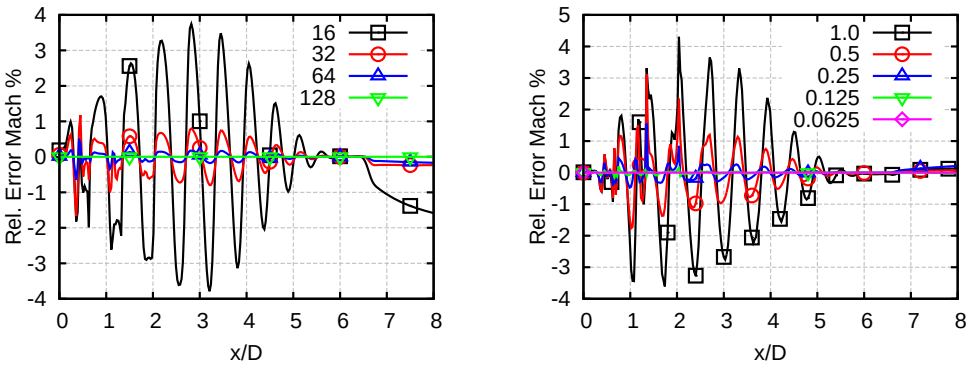

(a) (b)

Figure 2 Mach number profile relative error of the deterministic base case at the centreline for **(a)** different azimuthal discretizations, where each line represents the number of azimuthal nodes, and **(b)** different axial discretizations, where each line represents the starting position where the mesh is uniform. The refined mesh has been used as converged solution.

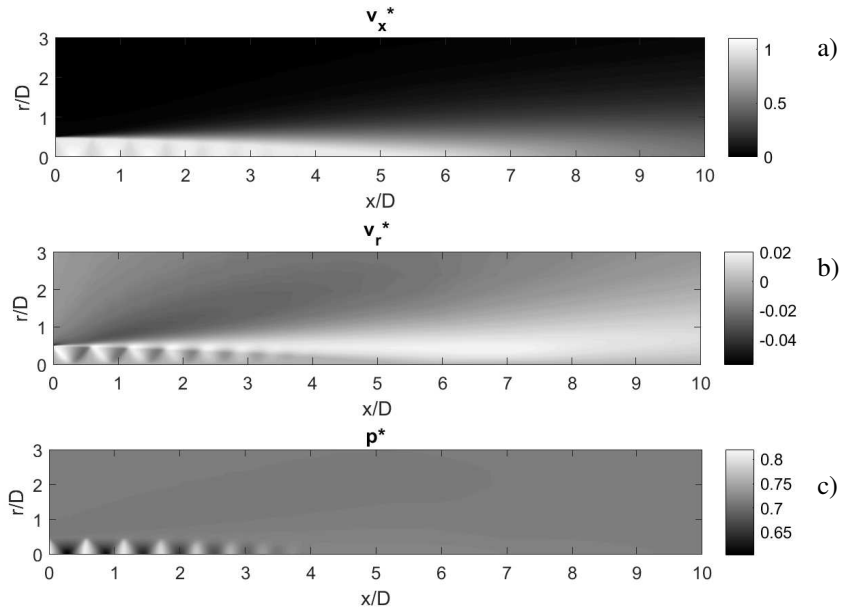

Figure 3 CFD RANS simulations of the deterministic base case of the under-expanded jet in ***elsA***. The shown parameters are (a) the dimensionless axial velocity, $v_x^* = v_x/c_{ref}$, (b) dimensionless radial velocity, $v_r^* = v_r/c_{ref}$ and (c) dimensionless static pressure, $p^* = \frac{p}{\gamma_{ref}\, p_{ref}}$, with $\gamma = 1.4$ the specific heat ratio, $p_{ref} = 98000\ Pa$ the reference pressure and $c_{ref} = 340.26\ m/s$ the reference speed of sound.

means of UQ, an assessment of the accuracy of the simulation can be done. To use a one-equation approach is also an advantage since, in uncertainty studies, the number of deterministic simulations to run is usually large and becomes a cheaper approach. It is well known [42] that

the S-A model needs improvement for subsonic jet flows however, Huang et al. [42] also showed that the one-equation model is the second best option after the $k-\omega$ model in terms of relative performances when tested in several subsonic academic cases. Moreover, the S-A model, gives the best numerical performance based on grid spacing required for accurate solutions and y^+ allowable at the first grid point off the wall. This is for sure a positive aspect of the model for UQ simulations when changes in uncertain parameters lead to changes in the boundary layer thickness. For supersonic flows such as the one of a supersonic jet in a transonic cross flow [70], even though the S-A model gives the worst results in terms of surface pressure, it gives the best agreement with experiments for the location and strength of vortical structures. Good agreement is also found for a supersonic under-expanded ejector [12] and a supersonic under-expanded impinging jet [4] for several turbulence models including the S-A model.

Nonetheless, different turbulence models have been tested for the base case to compare the validity of our choice. To this end, RANS simulations are performed with Fluent in the two-dimensional axisymmetric formulation. The Mach profiles at the centreline are shown in Fig. 4. Both codes give similar results for the S-A model in terms of shock-cell spacing and amplitude, but Fluent results give a shorter potential core. The $k-\varepsilon$ turbulence model gives similar shock spacing and amplitude as the S-A model, but it correctly captures the potential core. When comparing against the experimental results, the turbulence model $k-\omega$ gives the best results in terms of shock amplitude, but it overestimates the length of the potential core by more than 50%. Similar decays are found in the literature when using different turbulence models [28, 80, 1]. According to these results, the Spalart-Allmaras model has a similar performance than the other turbulence models with the advantage of having only one equation, and thus being numerically more efficient and less computationally expensive to simulate several cases for uncertainty quantification purposes.

3. Uncertainty Quantification on 3D RANS simulations

One of the drawbacks in RANS is to replicate turbulence-based features reliably. Therefore, to quantify the impact of inaccuracies in both the computational injection of turbulence and experimental jet performance is a plus. This provides extra metrics about the RANS simulation. For this task Uncertainty Quantification and Sensitivity Analysis methods are applied. In this section, the input uncertainties are described as well as the mathematical methods used for their handling.

3.1. Tests and Sources of Uncertainty

The parameters that are treated as stochastic inputs for uncertainty quantification are the stagnation pressure, p_s, and the turbulent to laminar viscosity ratio, $R_t = \mu_t/\mu$, and are both imposed at the inlet of the nozzle. These parameters have been selected because of their stochastic behaviour in nature. Other parameters could also be selected, but these are the most relevant ones according to our experience and some preliminary testing.

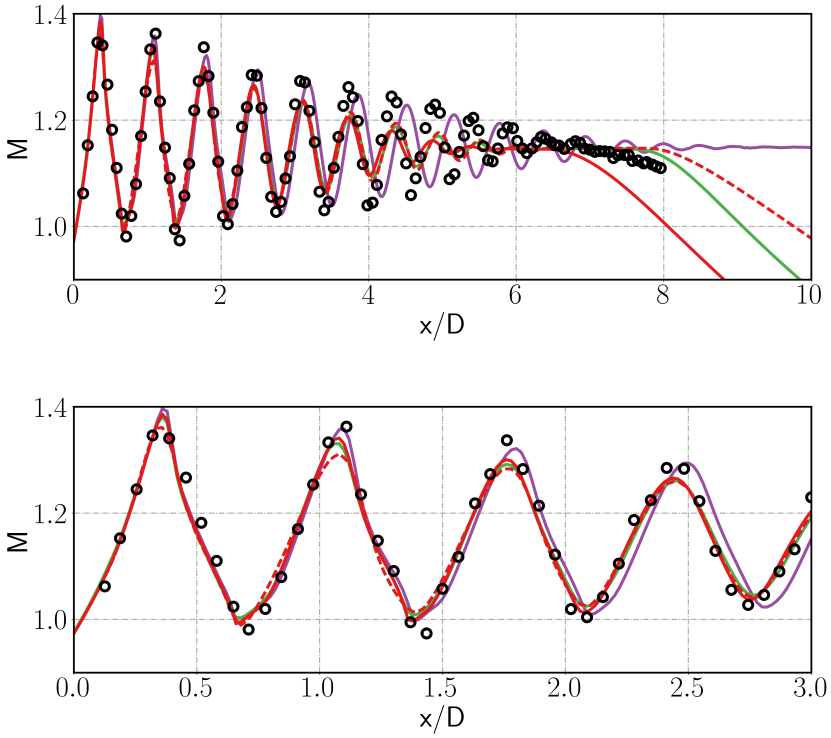

Figure 4 Mach number profile of the deterministic base case at the axis for different solvers and turbulence models. **(a)** full view, **(b)** detailed view. Red dashed line: 3D elsA, S-A. Red solid line: 2D-axi Fluent S-A. Green solid line: 2D-axi Fluent $k-\varepsilon$. Purple solid line: 2D-axi Fluent $k-\omega$. Symbols: Experimental data.

One of the greatest sources of uncertainty that one can recognise in these jet flows is the mass-flow rate, which is in fact related to other variables such as the nozzle diameter or stagnation pressure, being this flow parameter an interesting and relevant random input to replicate realistic conditions. Such decision was based on suggestions of experimentalists at von Karman Institute for Fluid Dynamics (VKI), a partner in our funded project. During a single experimental run, notable pressure variations are not yet expected due to emptying of the tanks. However, these are expected during repeated tests. This is because the membranes of the valves are opening and closing several times, and the displacements of these membranes can be slightly different for each run, leading to variations in the mass-flow rate. Moreover, one has to take into account the uncertainty of the measurement devices (pressure sensors).

As the test rig was not yet built to measure the stagnation pressure (p_s) uncertainty, it was agreed with the experimentalists to set a realistic range to compute the input uncertainty by a conservative variation of a ±5% by means of a uniform probabilistic distribution. The aim is, therefore, also to gain useful information, prior the first experimental test at VKI, by means of simulations. The same conservative approach was followed for the second source of uncertainty,

the laminar viscosity ratio (R_t), whose uncertainty was tested computationally. To sum up, the chosen probabilistic distribution is $p_s \sim U(0.95\bar{p}_s, 1.05\bar{p}_s) = U(211337, 233583)\ Pa$, where $\bar{p}_s$ refers to the deterministic base value $\bar{p}_s = 222460\ Pa$. For notation purposes in this paper, the variation coefficient from 0.95 to 1.05 will be also referred to as c_{p_s}.

As aforementioned, the second parameter is the laminar to turbulent viscosity ratio, $R_t = \nu_t/\nu$, used for the injection of turbulence in the Spalart-Allmaras model [89], which is in fact a computational input for the turbulence at the exit of the nozzle. This is more complicated to handle than the stagnation pressure, since there is no experimental benchmark data available for a calibration process, because this is a purely numerical. This parameter stays fixed when simulating the operating conditions of an experimental facility. However, dealing with it as a deterministic fixed parameter is not appropriate, as flow simulations are definitely sensitive to their set value and to quantify the change in the simulations is relevant. The variation of the parameter has been carefully chosen based on several tests on the CFD solver, for which the solution is close to subsonic experimental results (used as guidance since there are no supersonic experimental data available) even when it is largely varied.

According to the best practices proposed by Spalart & Rumsey [90], effective inflow conditions for the parameter R_t should lie within the range $(1, 10)$. However, simulations with higher values still give accurate predictions while increasing the convergence at high Reynolds numbers.

This lack of exactness in defining this parameter encouraged us to deal with it as an uncertainty source by means of an uniform probabilistic distribution. The CFD turbulent modelling by means of this parameter is not linked to any compulsory particular order of magnitude of this variable, and this freedom provides a very wide range of values that are almost equally valid without prior knowledge. This might seem a broad estimation, but the preliminary tests supported the idea. The chosen probabilistic distribution is $R_t \sim Unif(2.2, 220)$ where $R_t = 2.2$ is considered the deterministic base value as this was the value used by the authors in the initialisation of the flow for a Large Eddy Simulation [9]. Smaller values of R_t result in changes in the injection of turbulence too small to have an effect on the flow. On the other hand, by increasing this parameter at the inlet, it increases also the maximum dimensionless turbulent wall unit, y^+, achieved at the wall near the exit. Nevertheless, the y^+ remains of order unity changing from 1 to 6 for the highest R_t value. Figs. 5 and 6 show the Mach and R_t profiles for different R_t inlet values, respectively. Values greater than 220 are not part of the study as they present non-physical velocity profiles as shown in Fig. 7 for the axial velocity profile at $x = 2mm$, which are compared with the available experimental data. The values are non-dimensionalised by the maximum values due to the fact that the experimental data corresponds to a subsonic test case with a Mach number at the exit of the nozzle of $M_e = 0.9$.

Other random inputs were discarded. Feasible parameters suffering from uncertainty might be flow temperature or geometrical variations such as the diameter of the nozzle. Nevertheless, in order to notice some effect on the simulations, these variations must be remarkably greater than the expected variation effect (at least one order of magnitude). Other probabilistic distributions could be tested too. However, as the main goal is to be conservative prior any experimental tests at VKI and be aware of possible relevant variations in the quality of the jet flow computation,

the uniform distributions were the best choice. This modelling suggest that all inputs are equally likely to happen.

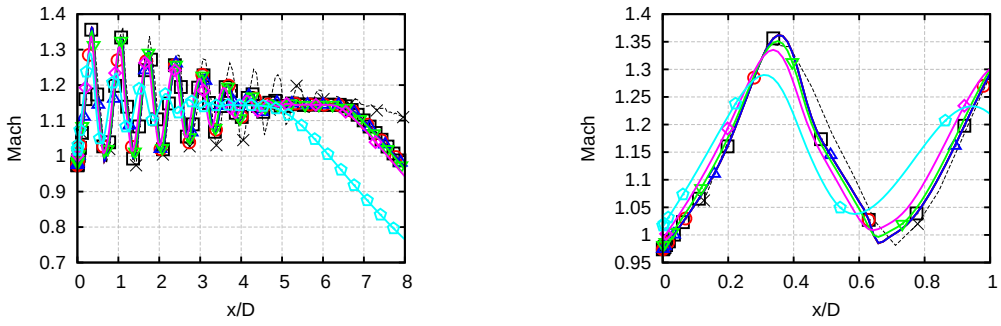

(a) (b)

Figure 5 Mach number profile of the deterministic base case at the centreline for different R_t inlet values in a (a) general and a (b) detailed view. Experimental ×, $R_t = 0.022$ □, $R_t = 0.22$ ○, $R_t = 2.2$ △, $R_t = 22$ ▽, $R_t = 220$ ◇, $R_t = 2200$ ⬠.

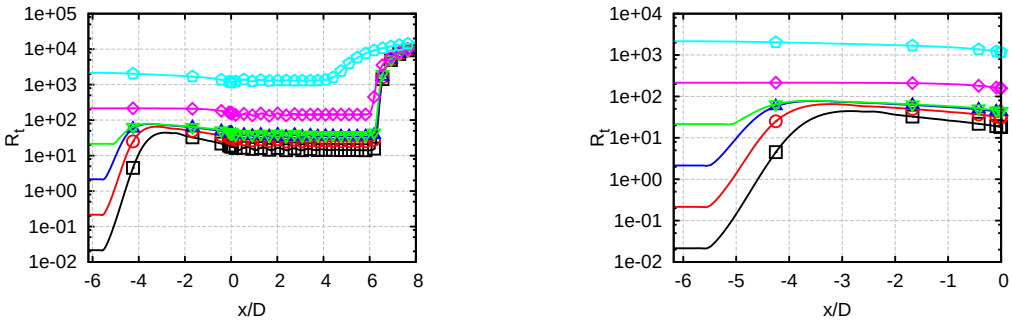

(a) (b)

Figure 6 R_t profile of the deterministic base case at the centreline for different R_t inlet values in a (a) general and a (b) detailed view. $R_t = 0.022$ □, $R_t = 0.22$ ○, $R_t = 2.2$ △, $R_t = 22$ ▽, $R_t = 220$ ◇, $R_t = 2200$ ⬠.

3.2. Uncertainty Quantification Methods: Generalised Polynomial Chaos and Kriging Surrogates

Uncertainty quantification (UQ) has become a very influential field, due to the fact that methods developed in the recent years bring the possibility of understanding how the behaviour of expensive (normally in terms of computation) mathematical models is being affected by imprecisely defined inputs. For a more formal description, let consider the differential operator on an output of interest of a stationary problem, $y(\mathbf{x}, \boldsymbol{\xi}(\eta))$ as

$$\mathcal{L}(\mathbf{x}, \boldsymbol{\xi}(\eta); y(\mathbf{x}, \boldsymbol{\xi}(\eta))) = Q(\mathbf{x}, \boldsymbol{\xi}(\eta)), \tag{3}$$

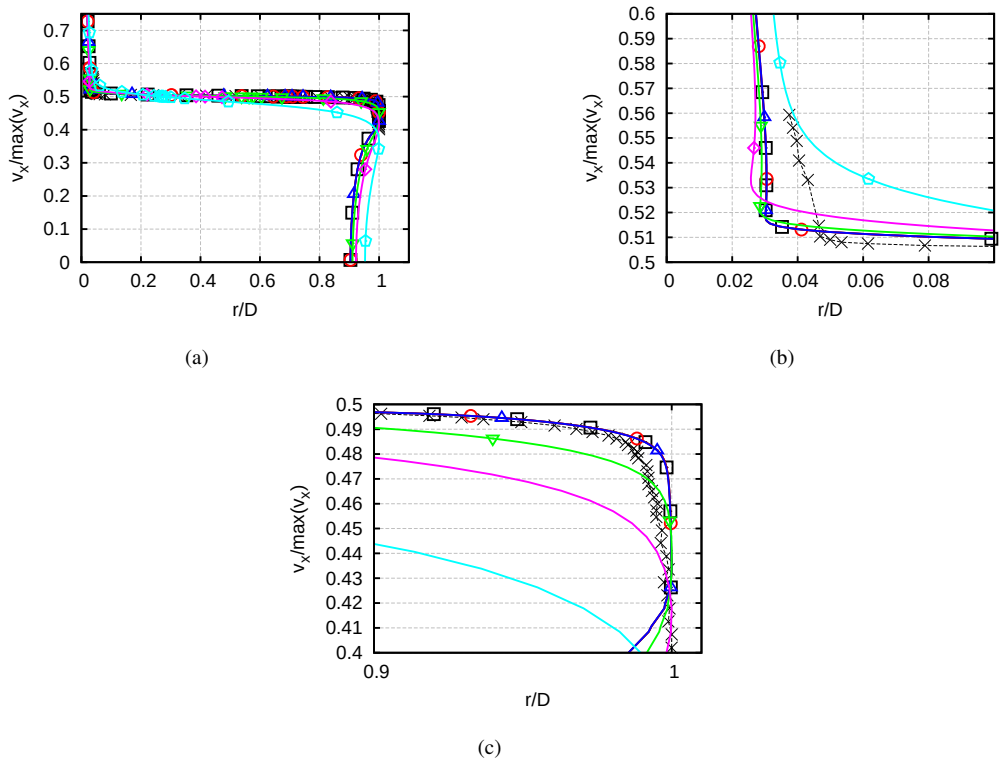

Figure 7 Axial velocity profile of the deterministic base case at the centreline for different R_t inlet values in a (a) general and a (b)&(c) detailed view. Experimental $\times$, $R_t = 0.022$ $\square$, $R_t = 0.22$ $\circ$, $R_t = 2.2$ $\triangle$, $R_t = 22$ $\triangledown$, $R_t = 220$ $\diamond$, $R_t = 2200$ $\pentagon$.

with $\mathcal{L}$ and $\mathcal{Q}$ the differential operators on $\mathcal{D} \times \Xi$, where $\mathbf{x} \in \mathcal{D} \subset \mathbb{R}^d$, $d \in \{1, 2, 3\}$. η denotes events in the complete probabilistic space $(\hat{\Omega}, \hat{\mathcal{F}}, \hat{P})$, with $\hat{\mathcal{F}} \subset 2^{\hat{\Omega}}$ the σ-algebra of subsets of $\hat{\Omega}$ and $\hat{P}$ a probability measure. $\Xi \subset \mathbb{R}^{N_\xi}$, is the stochastic space on which the random variables $\boldsymbol{\xi}(\eta)$ are defined and N_ξ stands for the number of random variables (two in our case under study).

The first approach presented in this section is the Polynomial Chaos method. This method has been developed to solve Stochastic Differential and Stochastic Partial Differential Equations (SDE and SPDE, respectively)[91]. It was first introduced by Wiener [104], in order to model stochastic processes through Hermite polynomials with Gaussian random variables. Lately, Xiu & Karniadakis extended the original version of Wiener to a wider family of basis functions leading to the known concept of generalized Polynomial Chaos (gPC) [107]. It is also known as Askey-Chaos, due to the fact that is formed by the complete set of orthogonal polynomials from the Askey scheme [10]. The objective of such extension is that for non-Gaussian random inputs, the convergence of the Hermite-chaos is low, and in some cases, disastrous.

Polynomial Chaos is a spectral method. Thus, an important advantage is that one may de-

compose a random representation into deterministic and stochastic components as

$$\hat{y}^{gPC}(\mathbf{x}, \boldsymbol{\xi}) = \sum_{j=0}^{\infty} y_{m_j}(\mathbf{x})\, \Psi_j(\boldsymbol{\xi}), \tag{4}$$

where y_{m_j} are the deterministic coefficients (also called modal coefficients) with $\mathbf{x} = (x, r)$ and $\Psi_j(\boldsymbol{\xi})$ is the orthogonal base, in a tensor-like form by 1-D products of the orthogonal polynomials, satisfying the orthogonality relation

$$\left\langle \Psi_i, \Psi_j \right\rangle = \left\langle \Psi_i^2 \right\rangle \delta_{ij}, \tag{5}$$

with δ_{ij} the Kronecker delta function and $\langle \cdot, \cdot \rangle$ the inner product. In Eq. (4), the expansion has infinite terms. For practical reasons, this expansion has to be truncated accounting $N_t - 1$ terms, with

$$N_t = \frac{(N_\xi + P)!}{N_\xi!\, P!} \tag{6}$$

and P standing for the maximum order of the expansion. The chaos expansion is finally expressed as

$$\hat{y}^{gPC}(\mathbf{x}, \boldsymbol{\xi}) = \sum_{j=0}^{N_t - 1} y_{m_j}(\mathbf{x})\, \Psi_j(\boldsymbol{\xi}). \tag{7}$$

In the following, $\mathbf{x}$ and $\boldsymbol{\xi}$ are removed in the notation for sake of simplicity. Polynomial Chaos can be an Intrusive or Non-Intrusive approach. In this paper it is implemented as Non-Intrusive, due to the fact that it takes into account the solver as a black-box not requiring to code inside the CFD software. This has been a popular method in recent years with many successful applications in the literature [17, 53, 27]. As the input uncertainties have been modeled by Uniform Probabilistic Distributions, Legendre polynomial basis functions are chosen. For the deterministic realisations required in the expansion, collocation points have to be carefully selected if one wants to reduce the number of model evaluations. Regarding the selection of the collocation point configuration, the use of tensor grids represents an expensive way. A much efficient mean is the use of sparse grids [87]. In this work, Clenshaw-Curtis (C-C) quadrature nested rule is applied [99] to generate the weights and nodes of the sparse grid. The coefficients y_{m_j} can now be computed as

$$y_{m_j} = \frac{\left\langle y, \Psi_j \right\rangle}{\left\langle \Psi_j^2 \right\rangle}. \tag{8}$$

The evaluation of Eq. (8) is in fact the computation of the multidimensional integral over the domain $\hat{\Omega}$, on which deterministic simulations of y from the CFD solver are set by the sparse grid. Moreover, this inner product is based on the measure of weights according to the choice of the orthogonal polynomials Ψ, as the weight function is in fact the probabilistic distribution function. As input uncertainty is modelled by uniform distributions, the spectral method turns into a

Polynomial Legendre Chaos. Once the coefficients are computed, the mean and the variance can be found by

$$\mathbb{E}(\hat{y}^{gPC}) = y_{m_0}, \tag{9}$$

$$\mathbb{V}(\hat{y}^{gPC}) = \sum_{j=1}^{N_t-1} y_{m_j}^2 \left\langle \Psi_j^2 \right\rangle. \tag{10}$$

An advantage of Polynomial chaos is that Sensitivity Analysis is straightforward from UQ analytics. This is discussed in Section 4.

The second approach is Kriging interpolation (also known as Gaussian Process regression and in this paper under the acronym KG). This method is an interpolation surrogate method to approximate sets of data. Despite the fact that surrogates can be also constructed via Polynomial Chaos Expansion, the main idea of using Kriging is to try another method for comparison purposes. It is also possible hence to test whether Kriging surrogates can have a reliable behaviour with only a budget of 65 deterministic simulations from collocation methods.

In essence, Kriging is a two-step process: first a regression function $f(\boldsymbol{\xi})$ is generated based on the data set, and from its residuals a Gaussian process $Z(\boldsymbol{\xi})$ is built, as can be seen in Eq. (11)

$$\hat{y}^{KG}(\boldsymbol{\xi}) = \hat{f}(\boldsymbol{\xi}) + Z(\boldsymbol{\xi}) = \sum_{i=1}^{k} \gamma_i f_i(\boldsymbol{\xi}) + Z(\boldsymbol{\xi}), \tag{11}$$

where $f(\boldsymbol{\xi})$ stands for the $k \times 1$ vector of basis regression functions $[f_1(\boldsymbol{\xi})\ f_2(\boldsymbol{\xi})...f_k(\boldsymbol{\xi})]$ and γ_i denotes the coefficients. Depending on the regression function, Kriging can appear with different names. Universal Kriging defines the trend function as a multivariate polynomial, as described in Eq. (11). Simple Kriging refers to the use of a known constant parameter as regression function, *i.e.* $f(\boldsymbol{\xi}) = 0$. A more popular version is Ordinary Kriging, which also assumes a constant but unknown regression function $f(\boldsymbol{\xi}) = \gamma_0$. Universal Kriging with a second order polynomial regression was our choice.

The Gaussian process $Z(\boldsymbol{\xi})$ is assumed to have mean zero and $cov(Z(\xi_i), Z(\xi_i')) = \sigma_p^2 R_c(\theta, \xi_i, \xi_i')$, where σ_p^2 is the process variance and $R_c(\theta, \xi_i, \xi_i')$ is the correlation model or spatial correlation function (SCF). In order to create an accurate Kriging surrogate it is important to pay attention to the correlation function. This function only depends on the distance between the two points ξ_i and ξ_i', and, for the general exponential case introduced in Eq. (12), also on p. The smaller the distance between two points, the higher the correlation and, hence, the more the Kriging predictor is influenced by the other. By the same token, if the distance is increased, the correlation drops to zero. For these reasons, it is not useful to put several data points together, as the prediction would not be influenced. Many correlations can be tried, but in the present work the generalized exponential worked very well and was the final choice. From Eq. (12), exponential ($p = 1$) and Gaussian ($p = 2$) correlations were not appropriate for the wave-like surrogates since during tests these showed some bumped areas in the spaces between collocation nodes.

$$R_c(\theta, \xi_i, \xi_i') = e^{-\theta|\xi_i - \xi_i'|^p} \tag{12}$$

The essential difference between the two methods suggested in this paper is that whilst gPC estimates the coefficients for the orthogonal polynomial basis functions chosen according to the input distributions, Kriging is assuming that the output of the black-box model due to input variable uncertainty behaves as realisations of a Gaussian random process. This Bayesian approach intends to find probabilistic distributions over the functions, which are updated for new observed data. The Gaussian distributions also permit to compute empirical confidence intervals that provide a guidance on the positions where one could put additional data to improve the fit. When applying Kriging, it is assumed that data is spatially autocorrelated and statistical properties are independent on exact locations [45]. Kriging is not an efficient choice for data with very abrupt changes or discontinuities. For further information on Kriging (Gaussian processes), the reader is suggested to see [74, 18]. To apply the method, functions from the Matlab toolbox DACE [52] have been used.

Since shock-cells could create wavy changes in some features, the generation of surrogates has been carefully tested. The best performance was observed for the general exponential correlation, whose results for complicated data sets at different x/D locations to be interpolated can be seen in Fig. 8. Note that the surrogates have a non-sharp shape, so it is not expected to have substantial erratic contributions in uncertainty quantification when sampling across inter nodal areas.

Once the Kriging surrogates are available, sampling techniques are affordable. Latin Hypercube Sampling [39] and Random Sampling Monte Carlo are widely used non-intrusive methods for propagation of uncertainty in models. These methods have been used for many applications in science and a vast literature can be found. Because of the more stratified sampling, Latin Hypercube is preferred in this work. In Sections 3.3 and 4, the application of sampling techniques and Sensitivity Analysis on Kriging surrogates is developed and a comparison between Kriging and gPC results is discussed.

3.3. Comparison and Discussion of Uncertainty Quantification Results

The first step for uncertainty quantification is to test the convergence of each method with our computational budget. The idea behind using two different methods with different procedures (Kriging surrogate by sampling and gPC by quadrature on collocation points) is to provide two different ways hopefully leading to the same conclusions. When focusing on more than one method, conclusions can be contrasted. If a second approach is giving similar outputs, a more reliable feedback is provided.

For this purpose, several samplings were tried on KG surrogates by Latin Hypercube Sampling (LHS) and the results were compared with the gPC expansion of 4^{th} order (as $N_\xi = 2$, only 21 terms are required in the expansion). The accuracy of the methods has been tested along the lipline for the dimensionless axial velocity, v_x^*, and along the centreline for the Mach number, as these are the most relevant parts of the jet (along the centreline the shock-cells are strong and preliminary tests revealed that the nozzle lipline could have a sensitive part for v_x^* variations). To compute the integrals for the statistical moments of gPC, a sparse grid of 65 collocation points based on Clenshaw-Curtis (C-C) nested rule was used (the 65 collocation points correspond to

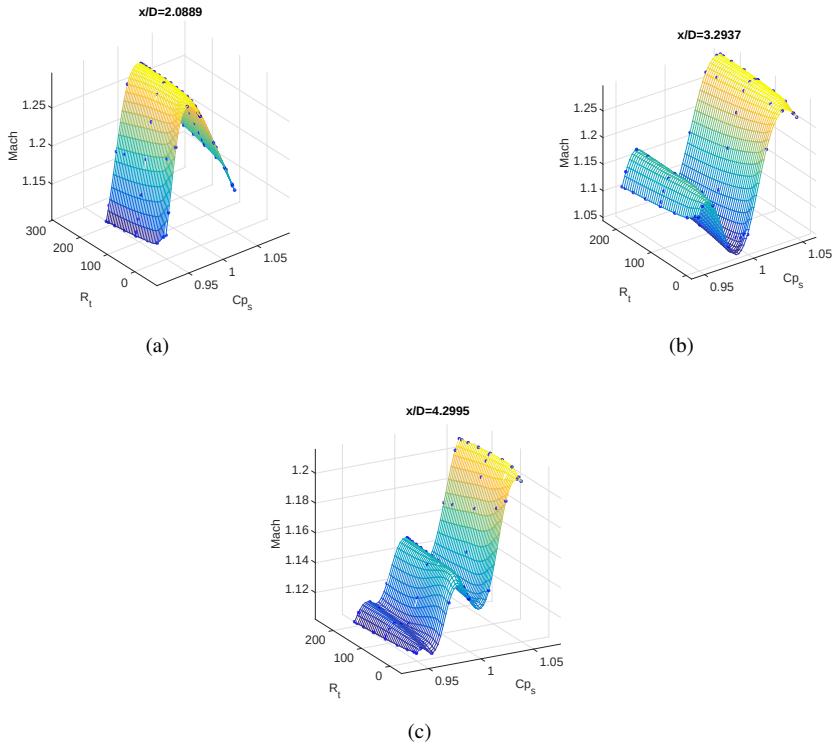

Figure 8 Examples of Kriging surrogates at several x/D distances on data sets with challenging shape. The blue points correspond to the deterministic CFD solutions from the fourth level of accuracy in the Clenshaw-Curtis sparse grid. In the plots c_{p_s} stands for the coefficient of variation for p_s ($\pm 5\%$).

the fourth level of accuracy), having a good match with Kriging sampled surrogates as shown in Figs. 9 and 10. The required number of collocation points was tested in [36], computing the convergence of statistical moments with Stochastic Collocation Method, so that level of accuracy of the sparse grid was intended here for gPC.

For convergence of gPC, the order of the expansion, P, and the number of collocation points, N_q, have to be controlled. If N_q is fixed to the fourth level of accuracy ($lvl4$) as aforementioned, it is now necessary to focus on the order of the expansion, P, to compute the statistical moments. These undergo convergence up to $P = 4$. However, if $P > 4$, divergence occurs and this is due to the fact that more collocation points are needed to compute the integrals. This has been tested numerically by means of generating artificial deterministic solutions from Kriging surrogates (see Fig. 11 and Table 1). With this procedure, the additional deterministic solutions of the sparse grid required for the fifth and sixth level of accuracy ($lvl5\,artif$ and $lvl6\,artif$ in the legend of the plots) are artificially generated and higher orders in the gPC expansion are tested. These plots are revealing that, in fact, in the region of $3 < x/D < 4$ more collocation points would be required with higher P. As for $lvl5$ and $lvl6$ are required 145 and 321 collocation points respectively with a not very relevant improvement in the accuracy, it is not worthy to perform such a large number

of simulations with the CFD code and *lvl*4 is assumed to be enough. Moreover, an adaptive refinement method [106] would not be worthy since the surrogates are different at each point of the domain.

Table 1 Since the initial budget was 64 points, and C-C sparse grid are nested, the additional collocation points for *lvl5 artif* and *lvl6 artif* are artificially generated from the Kriging surrogates.

C-C level of the sparse grid	Number of collocation points
lvl4	64
lvl5 artif	145
lvl6 artif	321

Regarding the convergence of sampling on Kriging surrogates, even with a reduced number of samples, converged statistical moments can be obtained. This is because LHS is a sampling strategy more efficient than Monte-Carlo and also due to the fact that the stochastic dimension is low, requiring to sample less dimensions.

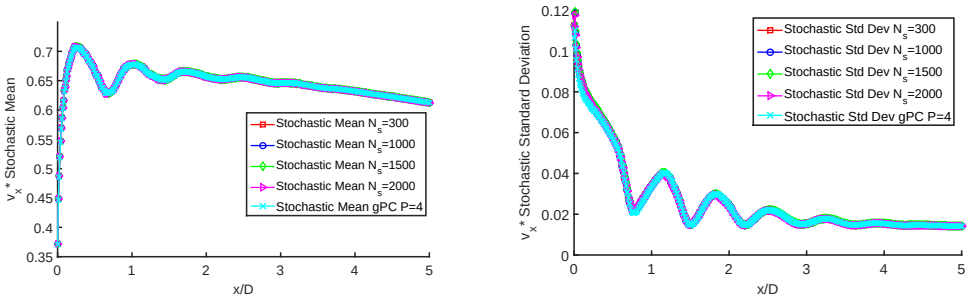

(a) (b)

Figure 9 Evolution of the v_x^* stochastic means (a) and standard deviations (b) along the lipline for LHS on Kriging surrogates with different number of samples, N_s, and its comparison with gPC results. Even for a small number of samples, LHS is undergoing very good convergence.

For the purpose of visualising uncertainty, the contour plots of the stochastic mean and variance are represented for both methods. In Figs. 12, 13 and 14 these values are plotted for v_x^*, v_r^* and p^* for Kriging surrogates only. The absolute error difference between KG and gPC is only shown for v_x^*, since for all variables such difference is negligible. Despite the absolute error in the variance can seem slightly notable, it is just illustrative. If attention is paid to v_x^* along the lipline close to the nozzle in Fig. 12.d, the absolute error seems to be notable, but in Fig. 9 the difference is practically negligible. The differences take place because surrogates are sampled with samples that do not take part in gPC analysis and, in gPC, statistical moments are obtained

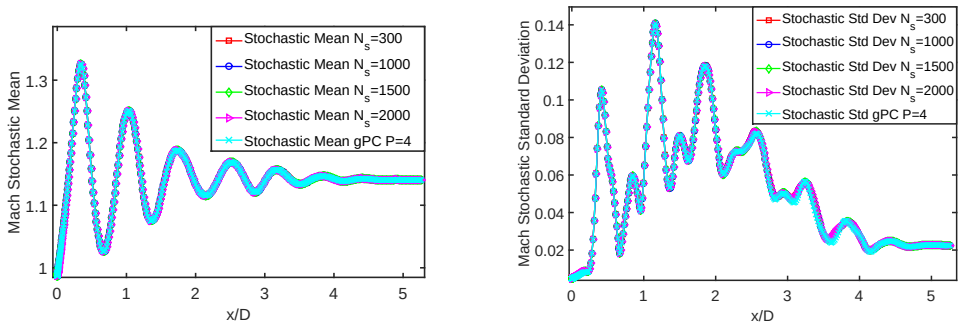

(a) (b)

Figure 10 Evolution of the Mach stochastic means (a) and standard deviations (b) along the centreline for LHS on Kriging surrogates for different number of samples and its comparison with gPC results. Even for a small number of samples, LHS is undergoing very good convergence.

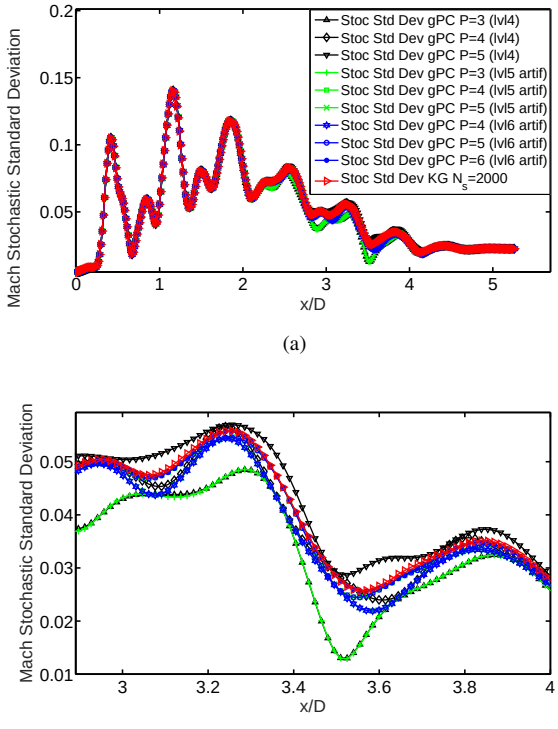

(a)

(b)

Figure 11 Evolution of (a) Mach stochastic standard deviation for different P and levels of the sparse grid and (b) a zoom of the hardest part in the convergence analysis. These results are compared with Kriging surrogates sampled by means of LHS with $N_s = 2000$.

by quadrature integrals, and not by sampling as in KG.

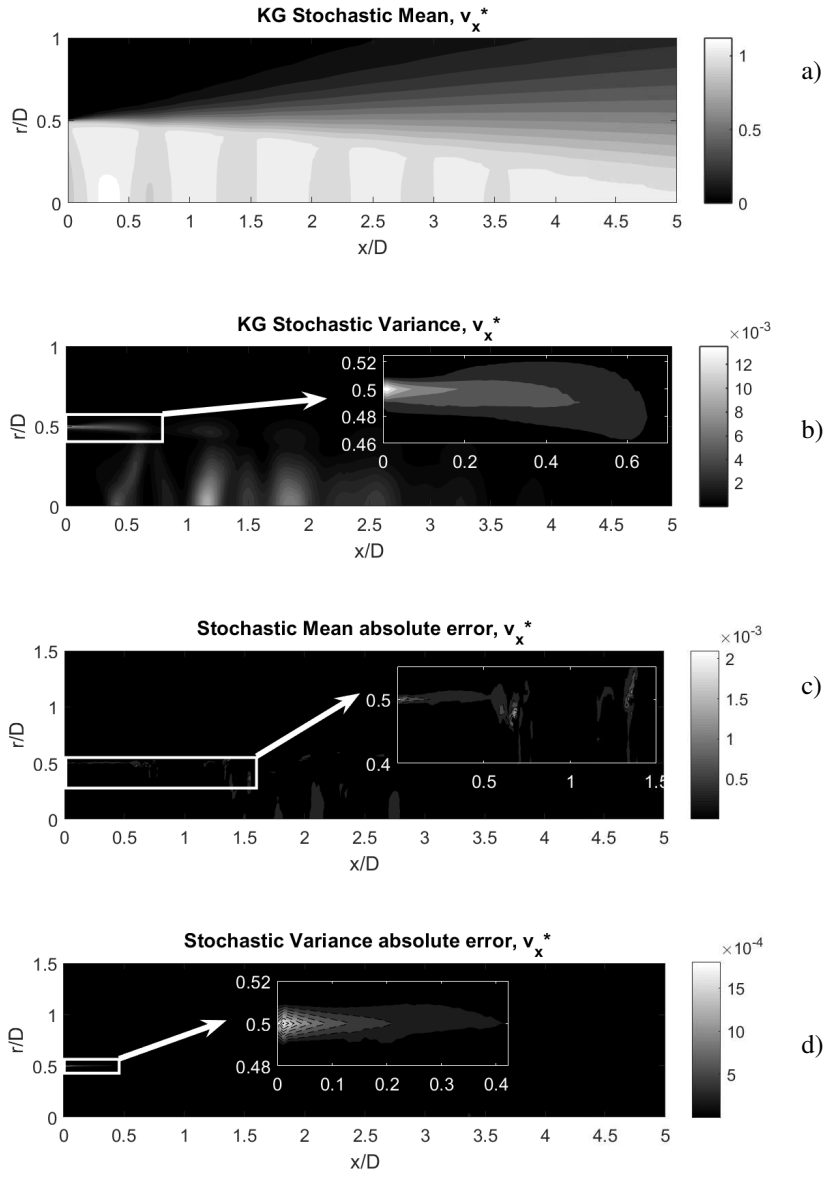

Figure 12 Contour plots of v_x^* (a) stochastic mean and (b) variance by means of LHS on KG surrogates. Contour plots of the absolute error between (c) stochastic mean and (d) variance between KG and gPC methods.

An objective of the analysis is to assess the simulation and to determine the regions of the jet

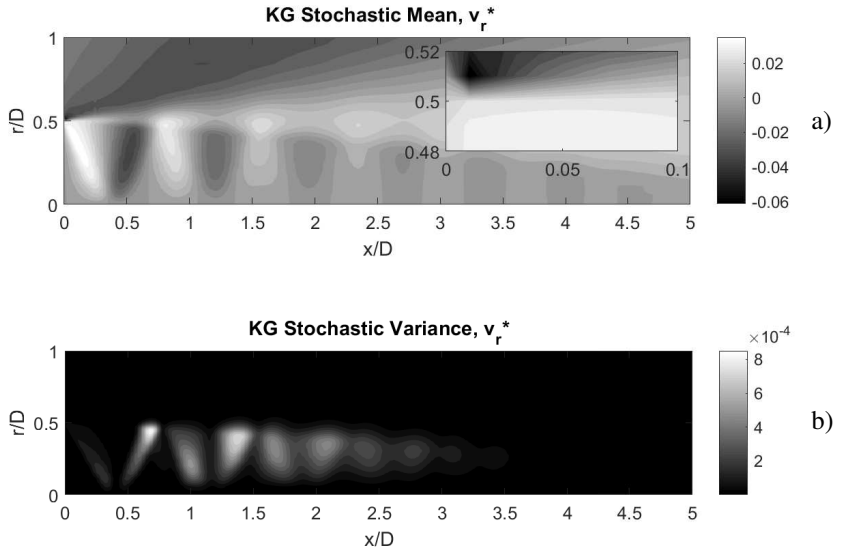

Figure 13 Contour plots of v_r^* (a) stochastic mean with detail of the nozzle lip exit and (b) variance by means of LHS on KG surrogates.

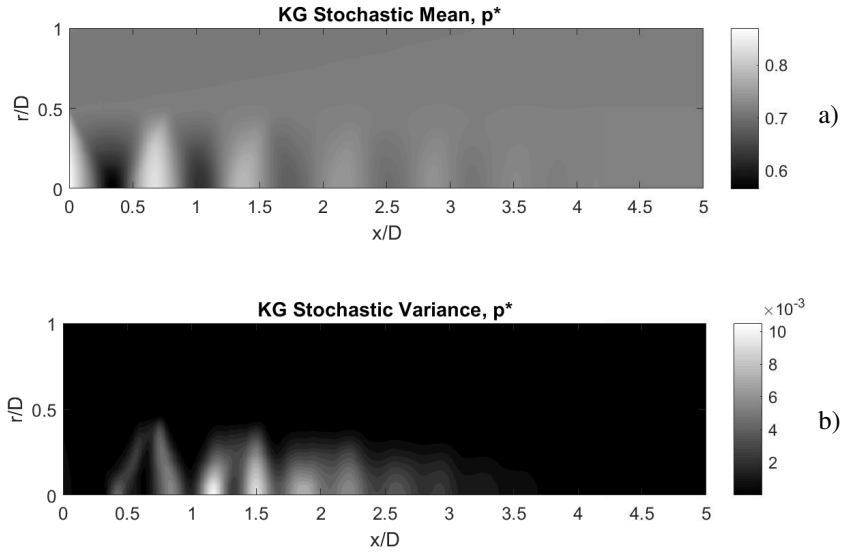

Figure 14 Contour plots of p^* (a) stochastic mean and (b) variance by means of LHS on KG surrogates.

prediction which are more sensitive to the input uncertainties. The spatial variation in uncertainty is not uniform across different quantities of interest. Diverse quantities exhibit diametric spatial sensitivity to input uncertainty. This has been suspected in the CFD community for a while [22], but no investigation has qualitative and quantitative proffered this before. From a careful analysis, one can draw the following conclusions.

For the dimensionless axial velocity, v_x^*, the most sensitive region is along the lipline, close to the nozzle lip (see Fig. 12.b). This uncertainty is in fact high, as can be observed in Fig. 16. Such large sensitivity nearby the nozzle lip makes sense due to the fact that small variations of the inner boundary layer at the exit of the nozzle could potentially modify the features that take place in the nozzle lip/lipline regions. It is observed that the percentiles are slightly far from the S-A deterministic case. This does not happen in the Mach number (Fig. 15), and the axial velocity at the lipline seems to be affected by the R_t calibration (the deterministic case corresponds to the lowest R_t value in the random input, being outside the plotted percentiles). This is actually obvious in the sense that the turbulence model has a dramatical impact on the shear-layer. The computation under uncertainty remarks that fact: even if R_t is chosen well enough according to the Mach number at the centreline, the axial velocity can be underestimated. It is, thus, important to look at the lipline if experimental or benchmark data is available for a proper calibration. Two-equation turbulence models data and LES [9] are used here for comparison as there is no experimental data available at the lipline, and only after $x/D = 3$ there is noticeable difference between LES and S-A results. To support the observations, the tests with R_t fixed at its deterministic value and cp_s varied at its minimum and maximum are shown. Also the test when cp_s fixed at its deterministic value and R_t maximum. When R_t minimum, that is the deterministic simulation (with lower values of $R_t = 2.2$ the v_x* does not change). It is guessed that the influence of the large values of R_t with p_s generate the lower values of v_x*. Also, when p_s is large, it is obvious that the amplitude of v_x* is increased.

A good test could be to try a lognormal distribution for R_t, and check how the percentile plot changes. However, since the objective of this work is simply to observe the sensitivity under equal probability (most conservative case scenario), it is discarded. It is recalled that in the initial seek for values for R_t, the jet performance was slightly perturbed for one or two orders of magnitude in the change. In UQ applied to higher fidelity simulations (*e.g.* Large Eddy Simulations, LES, not affordable here) it would be interesting to observe whether similar parametric uncertainty from the computation of turbulence intensity has an influence on the perturbations in the shear layer that lead to the feedback loop for screech noise [67]. Along the centreline, some uncertain regions can also be detected, but these can be better addressed when describing the variance in p^*.

Regarding the dimensionless radial velocity, v_r^*, the most sensitive region is immediately below the lipline (see Fig. 13.b). It can also be observed that the second and third shock-cell compression are notoriously the most sensitive to input uncertainty. Although jet noise is not studied in this paper because the available jet aeroacoustics models are not yet entirely reliable in RANS, screech jet noise is usually generated in that zone [66].

For the dimensionless static pressure, p^*, the most sensitive region is along the centreline (see Fig. 14.b). This is also observed for the Mach number in Fig. 15, where it can also be noticed

some uncertainty in the position of the shocks. The percentile envelopes show a variation in both the amplitude and position of the shock-cell, which makes sense due to the fact that shocks have a strong relation with the variations in stagnation pressure, according to basic fluid dynamics of compressible flows. The prescribed uncertainties would, as expected, be affecting the robustness of the simulated case scenario. In this figure, the percentile envelopes show that, despite the fact that the CFD RANS with Spalart-Allmaras (deterministic simulation) was not the most accurate model, the percentile envelopes are able to cover the most relevant data (first four shocks-cell bumps). This is interesting, since RANS simulations struggle to undergo a good match with experiments (especially in high-speed flows with shocks and eddy-viscosity turbulence models). The non enveloped data are possibly not remarkable outliers if experimental error bars are included (not reported in [5]). In addition, the changes in the position of the shock-cells are well featured. However, it can be observed that the oscillatory pattern is dissipated downstream, as consequence of the variations in the shock-cell positions (bump effect widen) because of uncertainty sources and the difficulty in RANS simulations to reproduce a realistic jet potential core. It is interesting to point out that even LES data [9] has problems to match experimental data, especially after the third shock-cell.

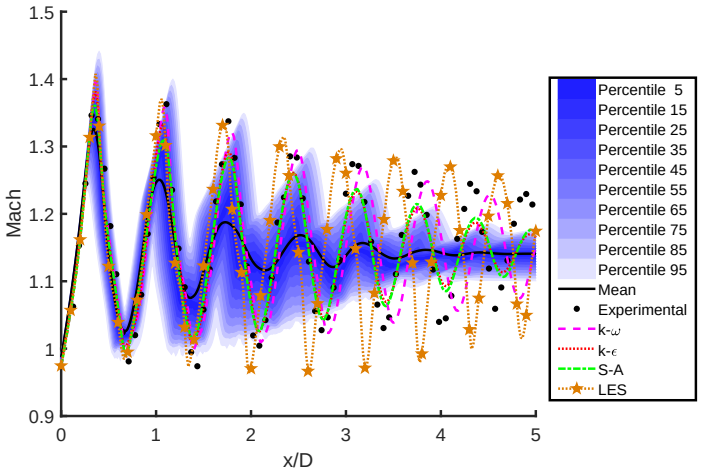

Figure 15 Percentiles from KG surrogates sampled by means of LHS with $N_s = 2000$ samples.

4. Global Sensitivity Analysis by Means of Generalised Polynomial Chaos and Kriging Surrogates

4.1. Principle of the Global Sensitivity Analysis

As explained in Section 1, an extension of UQ is the global Sensitivity Analysis. There are different methods for global Sensitivity Analysis, such as Screening Method, Derivate Based

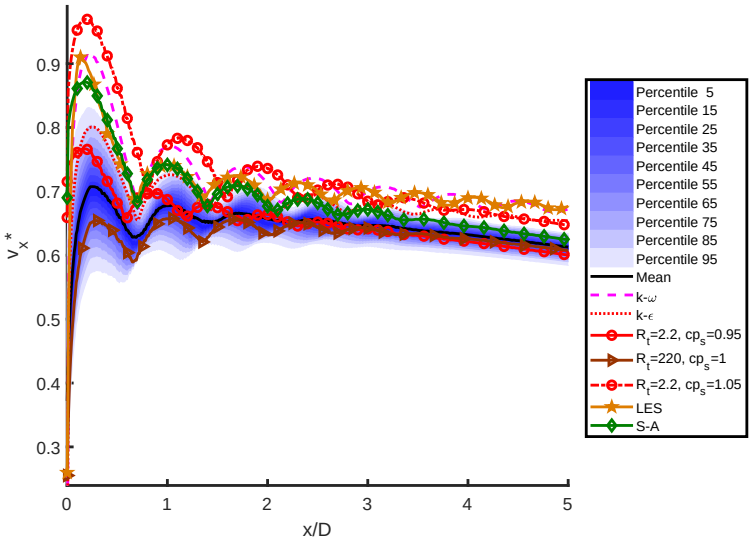

Figure 16 Percentiles from KG surrogates sampled by means of LHS with $N_s = 2000$ samples. LES data from [9].

Sensitivity Analysis or Variance-Based Analysis [95]. The scientist must choose appropriately depending on the computational cost, dimension of the problem or the expected output, amongst others. For the purposes of this work, a Variance-Based Analysis has been chosen [77]. One of the main reasons of using this method is the possibility of ranking the influence of the input factors by sensitivity indices.

The ANOVA decomposition of the variance is shown in Eq. (13), and sensitivity coefficients are computed from Eq. (14) from its proportion with respect to the total variance. S_i and S_{T_i}, in Eq. (15), are the first-order and total sensitivity index respectively. In the following equations the multiple subscripts refer to second, third or higher order interactions, depending on the number of subscripts. Given a model of the form $y = \hat{y}(\xi_1, \xi_2, ..., \xi_k)$, with y a scalar, the decomposition of the total variance, $\mathbb{V}(y)$, can be written as

$$\mathbb{V}(y) = \sum_{i=1}^{N_\xi} \mathbb{V}_{\xi_i} + \sum_{i=1, j>i}^{N_\xi} \mathbb{V}_{\xi_{ij}} + \sum_{i=1, k>j>i}^{N_\xi} \mathbb{V}_{\xi_{ijk}} + \dots . \tag{13}$$

The right hand side terms are the first and higher order contributions to the total variance. Dividing by the total variance, the sensitivities can be computed as

$$1 = \sum_{i=1}^{N_\xi} S_i + \sum_{i=1, j>i}^{N_\xi} S_{ij} + \sum_{i=1, k>j>i}^{N_\xi} S_{ijk} + \dots + S_{ijk,\dots,N_\xi}. \tag{14}$$

This leads to the following expresion for the total sensitivity index for the i-th parameter

$$S_{T_i} = S_i + S_{ij} + S_{ijk} + ... + S_{ijk...m} \tag{15}$$

and the associated sensitivity measure (first order sensitivity coefficient) is computed as

$$S_i = \frac{\mathbb{V}_{\xi_i}(\mathbb{E}_{\xi_{\sim_i}}(y|\xi_i))}{\mathbb{V}(y)}, \tag{16}$$

where ξ_i is the i-th factor and $\xi_{\sim_i}$ denotes the matrix of all factors but ξ_i. This index indicates by how much one could reduce on average the output variance if a parameter could be fixed. On the other hand, the total effect index can be computed as

$$S_{T_i} = \frac{\mathbb{E}_{\xi_{\sim_i}}(\mathbb{V}_{\xi_i}(y|\xi_{\sim_i}))}{\mathbb{V}(y)}. \tag{17}$$

S_{T_i} measures the total effect, *i.e.* first and higher order effects (interactions) of factor ξ_i. It represents a good measure to determine if a parameter is influential or not, and whether could be neglected from the model. The use of this sensitivity technique can be seen in many fields such as solar energy [81], wastewater treatment [84] or heat exchangers [31].

As the sensitivity indices are related to UQ, the approaches described in Section 3 are used in this section as well. Particularly, the Kriging surrogates are sampled according to [44] and the coefficients from gPC are used to compute the sensitivity indices. Despite that sampling could also be done on the Polynomial Chaos Expansion, it is important to note that a second objective in this work is to have two different methodologies to achieve the same results (sampling and quadrature based approaches). It has been proceeded in this way due to the fact that one of the interesting features of gPC is the possibility to perform Sensitivity Analysis straightforward after uncertainty quantification. For such task, it is not difficult to realise that there is a clear relation between Eqs. (10), (13) and (14). Eq. (10) that can be rewritten as

$$1 = \frac{1}{\mathbb{V}(\hat{y}^{gPC})} \sum_{j=1}^{N_t-1} y_{m_j}^2 \left\langle \Psi_j^2 \right\rangle, \tag{18}$$

and the first and higher-order sensitivity indices can carefully be extracted from the expression above since the literal part of each monomial gives the hints of the interaction.

Regarding the Kriging surrogates, $\hat{y}^{KG}$, as they are available from the former uncertainty analysis, it is now possible to compute the sensitivity indices from Eqs. (16) and (17). In order to compute S_i, ξ_i has to be fixed in several points $\xi_i = \xi_i^*$ along the possible values of the random variable and compute the mean individually for a further computation of $\mathbb{V}_{\xi_i}$. This would require a very large number of calculations since the number of fixed points has to be great enough to compute reliable statistics. A less expensive method has been coded in Matlab by following the procedure suggested in [44]. With this method, the first order sensitivity with Kriging surrogates,

S_i^{KG}, and the total effect, S_{Ti}^{KG}, can be computed as

$$S_i^{KG} = \frac{1 - \frac{1}{2N_s} \sum_{j=1}^{N_s} \left(\hat{y}^{KG}(B)_j - \hat{y}^{KG}(AB^i)_j \right)^2}{\mathbb{V}(\hat{y}^{KG})}, \tag{19}$$

$$S_{Ti}^{KG} = \frac{\frac{1}{2N_s} \sum_{j=1}^{N_s} \left(\hat{y}^{KG}(A)_j - \hat{y}^{KG}(AB^i)_j \right)^2}{\mathbb{V}(\hat{y}^{KG})}. \tag{20}$$

In these expressions, $\hat{y}^{KG}(A)$, $\hat{y}^{KG}(B)$ and $\hat{y}^{KG}(AB)$ are matrices that contain model evaluations, product of decomposition of the original matrices which contain the sample campaign. These two original matrices, A and B, correspond to two different independent samples onto the same surrogate and random variables, with $N_s \times N_\xi$ dimensions. Eqs (19) and (20) are built upon the original sensitivity indices shown in Eqs (16) and (17). These numerators come from the known identity

$$\mathbb{V}(y) = \mathbb{V}_{\xi_i}(\mathbb{E}_{\xi_{\sim_i}}(y|\xi_i)) \; + \; \mathbb{E}_{\xi_i}(\mathbb{V}_{\xi_{\sim_i}}(y|\xi_i)). \tag{21}$$

A formal definition of the method requires some mathematical background in statistics and will not be included in this section. The reader is referred to [44, 35] for further details. However, for the sake of practical clarification, the procedure developed on the surrogates is broken down as follows:

1. Generate two independent Design of Experiment with LHS: A and B.
2. For the i-th sensitivity index, only the i-th column in matrix A is swapped with the i-th column in matrix B. The new matrix is referred to as AB^i. This new version of the A matrix clearly preserves its $N_s \times N_\xi$ structure and can still be considered a sample matrix, but without the original properties of a LHS.
3. Evaluate the Kriging surrogates with the elements from the matrices A, B and AB^i.
4. Compute the sensitivity coefficients in Eqs. (19) and (20). j stands for the row of the matrices.

This alternative approach dramatically decreases the number of model evaluations in comparison to brute force method.

4.2. Discussion of Global Sensitivity Analysis Results

Since uncertainty quantification results are compared by means of Kriging surrogates and Polynomial Chaos in Section 3, attention is now paid on the sensitivity contours for the dimensionless static pressure, p^*, plotted in Fig. 17.

One of the motivations of using two methods for Sensitivity Analysis purposes is that the resulting contours for the sensitivity indices were not intuitive, which could be product of errors when implementing the codes. Fortunately, both methods provided similar solutions, discarding that. The explanation behind the contours appearance is that sensitivity is quantified simply providing a 'ratio' of contribution to uncertainty at every point of the CFD domain with respect

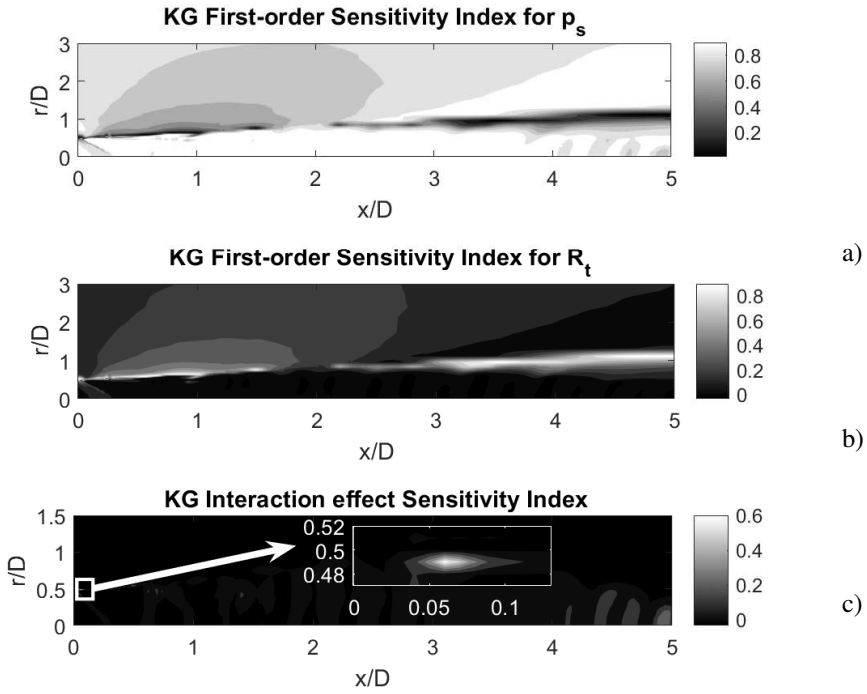

a)

b)

c)

Figure 17 Sensitivity indices contour plots by means of Kriging for p^*. a) and b) are the first-order sensitivities and c) higher-order interaction.

to the total variance at such point. A solution to provide a more intuitive and useful insight is to show the contribution to the total variance by each parameter as shown in Figs. 18-20. For representation of the quantities of interest, now only gPC results will be shown, as the difference between both gPC and KG was checked and found to be negligible.

Similarly for uncertainty quantification, in this section several interesting patterns have been observed and some conclusions have been drawn.

For the dimensionless axial velocity, v_x^*, the most sensitive region was detected along the lipline, close to the nozzle lip (see Fig. 12.b). The associated uncertainty is mainly due to the imprecision in the laminar to turbulent viscosity ratio, R_t, from the Spalart-Almaras turbulent model (see Fig. 18.b). Therefore, it is envisaged that a proper selection of the S-A parameter has only influence in the initial part of the lipline. One could also expect a remarkable sensitivity along the lipline or spreading angle associated to R_t because of the propagation of uncertainty in the downstream simulation of a turbulent jet, but it has not been observed such sensitivity with RANS. The stagnation pressure uncertainty, p_s, is also playing an influential role (Fig. 18.a), but its impact is not as high as by R_t in the area immediately at the nozzle exit. The contribution to uncertainty in the shock-cell areas close to the axis is done only by means of p_s uncertainty. The higher-order effect is not relevant.

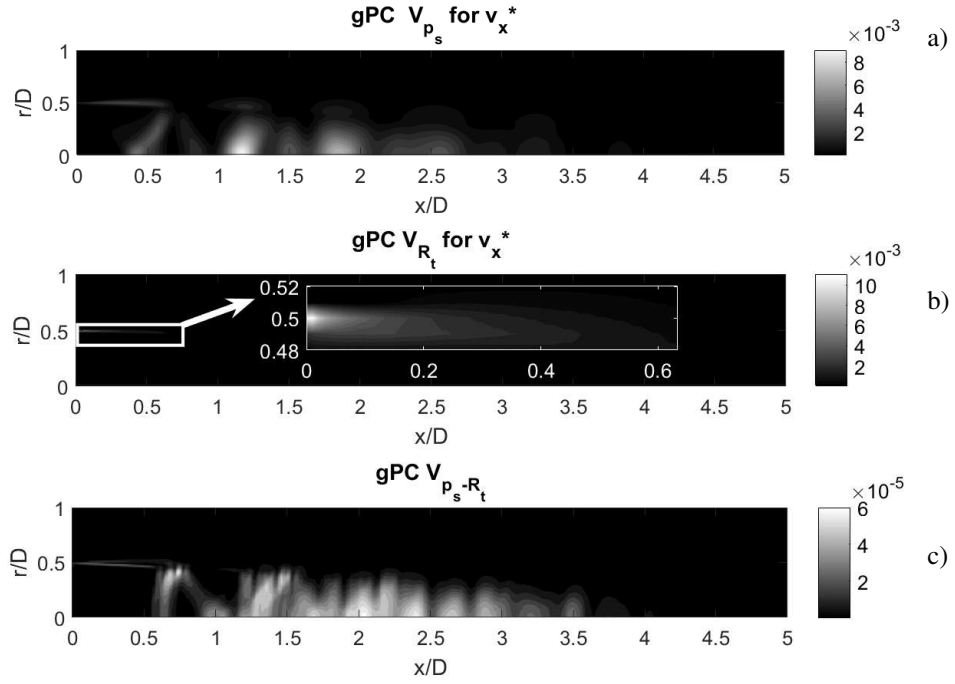

Figure 18 Contribution to the total variance of a) stagnation pressure, b) laminar to turbulent viscosity ratio and c) their interaction, for v_x^*.

Regarding the dimensionless radial velocity, v_r^*, the most sensitive region is immediately below the lipline (see Fig. 13.b). This uncertainty is undoubtedly linked to p_s as seen in Fig. 19.a, and its value is weak. The effect of R_t has no noticeable influence.

For the dimensionless static pressure, p^*, the most sensitive region is along the centreline (see Fig. 14.b). As can be seen in Fig. 20.a, p_s uncertainty is again the most influential one, and the influence of R_t uncertainty is practically null. Closer to the lipline, R_t uncertainty is greater, but not very significant. The reason of the dotted pattern related to R_t variance, also present in v_r* contours, is not clear.

5. Conclusions

The main objective of this analysis is to assess computationally the impact of uncertainties in the simulation of an under-expanded jet flow with shock-cells from an aircraft exhaust by means of RANS simulations with the Spalart-Allmaras turbulent model. Simulated data is compared to $k-\epsilon$ and $k-\omega$ eddy-viscosity models, LES data and experimental data. This pretends to expand the views of the popular deterministic approaches in RANS, which can lead to less reliable conclusions from simulations. As the Spalart-Allmaras turbulent model does not provide usually a good performance in compressible jet flows (it is a one-equation eddy viscosity model), efforts are focused on the analysis of the simulation. Experimental uncertainty is also present in the

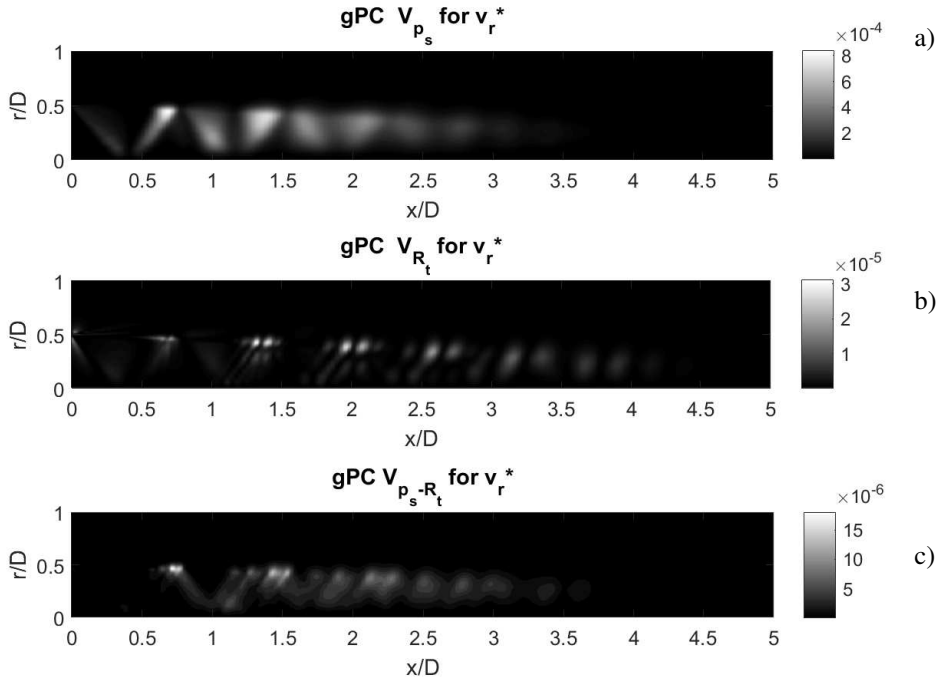

Figure 19 Contribution to the total variance of a) stagnation pressure, b) laminar to turbulent viscosity ratio and c) their interaction, for v_r^*.

computations, and by means of sensitivity analysis, the influence of each source of uncertainty can be ranked and isolated. This analysis represents first numerical study that provides evidence for the non-uniformity in spatial sensitivities of the quantities of interest to input uncertainty in simulations of jet flows.

Specifically, Non-Intrusive Uncertainty Quantification techniques have been applied to 3D RANS CFD simulations of a supersonic under-expanded jet. The computational analysis accurately simulates the most relevant shock-cells with the Spalart-Allmaras turbulence model, in order to understand how the impact of input uncertainty (experimental and in turbulence modelling) affects to the simulated flow properties. A global Sensitivity Analysis was also carried out to understand the relevance of each random input separately in the output uncertainty. The results from the application of both methods (generalised Polynomial Chaos with quadrature and Kriging with Latin Hypercube Sampling) were identical.

Large Eddy or Direct Numerical Simulations are unaffordable for uncertainty quantification in shock-cell noise, and the use of RANS remains a recommended procedure in industry to measure the impact of uncertainties in the computation of the jet flow. From the analysis on the CFD simulations, the following conclusions can be drawn.

Firstly, despite the fact that shock-cells could be problematic in catching features in uncertainty quantification, convergence was achieved with only 65 collocation points from a Clenshaw-Curtis sparse grid. The shape of the Kriging surrogates looks appropriate to interpolate the train-

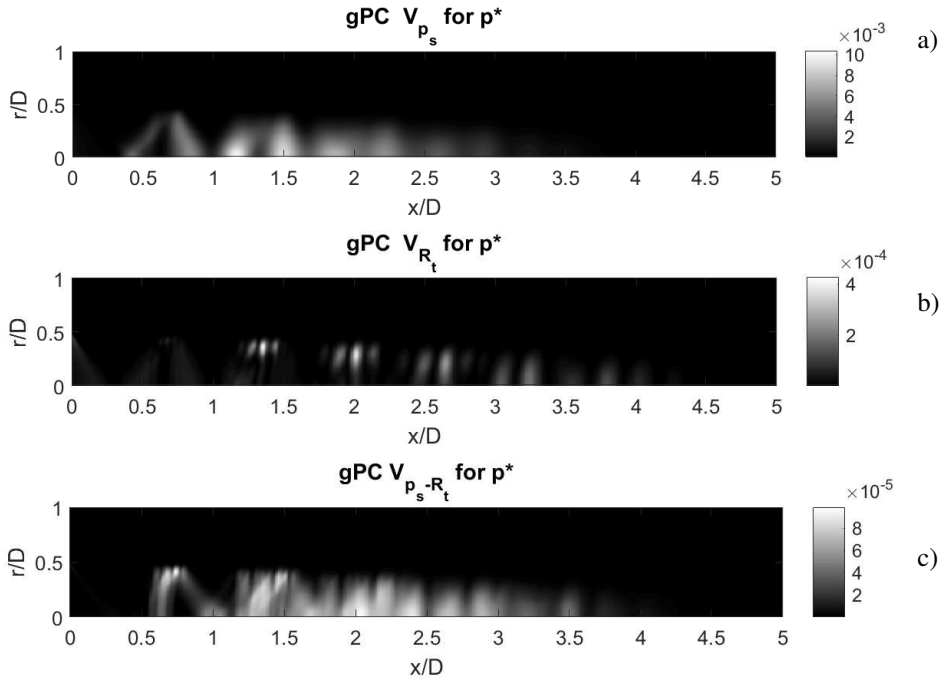

Figure 20 Contribution to the total variance of a) stagnation pressure, b) laminar to turbulent viscosity ratio and c) their interaction, for p^*.

ing data, as convergence was achieved, providing also the same results as Polynomial Chaos.

The variance in the Mach number is set by the contribution of the stagnation pressure uncertainty. The connection is clear from basic fluid dynamics, but the relatively low impact of large R_t uncertainty is of interest, since a bad calibration of such parameter may not be affecting the jet flow simulation notably. This low effect of R_t in central parts of the jet was also noticed in the contour plots of the variance in v_x^* and v_r^*. In addition, the experimental data of the Mach number along the centreline was well matched by the uncertainty envelopes.

The area immediately after the nozzle lip is highly sensitive to input uncertainty, especially from R_t, partly because of the difficulty to simulate this zone. This outcome is observed in the variance of v_x^*, where this behaviour can be product not only of turbulence sensitivity, but also the pressure suction effect. Anyway, uncertainty in that region is something interesting to take into account, as this is the beginning of the shear-layer development. It is envisaged that R_t variation is actually dramatically affecting v_x* along the lipline, with the percentile envelopes far from LES data used as reference, as well as the two-equations turbulence models in RANS. Low values of R_t provided very similar results to LES for the $x/D < 3$ area. Some light contributions to uncertainty have been noticed along the lipline for the radial velocity, v_r^*.

To summarise, the simulation of single under-expanded jets by means of RANS with the Spalart-Allmaras turbulence model looks an appropriate alternative to other more expensive methods if its accuracy is assessed by an uncertainty quantification framework. Future work

would be a plus on UQ applied to higher fidelity simulations, unaffordable yet for such computationally demanding task. Also noise emission uncertainty can be an additional scope not achievable with sufficient accuracy by means of the current jet noise models available for RANS simulations.

Acknowledgments

This research project is supported by the Marie Curie Initial Training Networks (ITN) AeroTraNet 2 of the European Community's Seventh Framework Programme (FP7) under contract number PITN-GA-2012-317142 that aimed to generate a ready to use model for shock-cell noise characterization. The authors are thankful to Onera for licensing CERFACS to use the code ***elsA***, to Daniel Guariglia and Christophe Schram (von Karman Institute for Fluid Dynamics) for the discussions about experimental uncertainty and to Prof. Stéphane Moreau for the resources offered to run Fluent simulations. The authors also acknowledge the anonymous reviewers for their useful comments and suggestions on this paper.

References

[1] Abdelhamid, Y. A., Ganz, U. W., 2007. Prediction of shock-cell structure and noise in dual flow nozzles. AIAA Paper 3721, 2007.

[2] Adya, S., 2011. Uncertainty quantification integrated to computational fluid dynamic modeling of synthetic jet actuators.

[3] Alonso, J. J., Fenrich, R., Menier, V., Iaccarino, G., Mishra, A. A., Eldred, M. S., Jakemann, J., Constantine, P., Duraisamy, K., 2017. Scalable environment for quantification of uncertainty and optimization in industrial applications (SEQUOIA). In: 19th AIAA Non-Deterministic Approaches Conference. p. 1327.

[4] Alvi, F., Ladd, J., Bower, W., 2002. Experimental and computational investigation of supersonic impinging jets. AIAA Journal 40 (4), 599–609.

[5] André, B., 2012. Etude expérimentale de l'effet du vol sur le bruit de choc de jets supersoniques sous-détendus. Ph.D. thesis, L'École Centrale de Lyon.

[6] André, B., Castelain, T., Bailly, C., 2013. Broadband shock-associated noise in screeching and non-screeching underexpanded supersonic jets. AIAA Journal 51 (3), 665–673.

[7] Ansaldi, T., Airiau, C., 2015. Sensitivity analysis for subsonic jet using adjoint of non local stability equations. In: 21st AIAA/CEAS Aeroacoustics Conference, Dallas TX, USA.

[8] Ansaldi, T., Granados-Ortiz, F.-J., Airiau, C., Lai, C.-H., 2015. Sensitivity and Uncertainty Quantification for Jet Noise Analysis. In: 22ème Congrès Français de Mécanique 2015, organised by L'Association Française de Mécanique. Lyon (France). 24-28th August 2015.

[9] Arroyo, C. P., Daviller, G., Puigt, G., Airiau, C., Moreau, S., 2018. Identification of temporal and spatial signatures of broadband shock-associated noise. Shock Waves, 1–18.

[10] Askey, R., Wilson, J., 1985. Some basic hypergeometric polynomials that generalize Jacobi polynomials, vol. 319. Mem. Amer. Math., Providence, RI.

[11] Bernardini, E., Spence, S. M., Wei, D., Kareem, A., 2015. Aerodynamic shape optimization of civil structures: A CFD-enabled Kriging-based approach. Journal of Wind Engineering and Industrial Aerodynamics 144, 154–164.

[12] Besagni, G., Mereu, R., Colombo, E., 2014. Cfd study of ejector efficiencies. In: ASME 2014 12th Biennal Conference on Engineering Systems Design and Analysis, Vol. Dynamics, Vibration and Control. p. V02T11A004.

[13] Cambier, L., Heib, S., Plot, S., 2013. The Onera elsA CFD software: input from research and feedback from industry. MI 14 (03), 159–174.

[14] Carnevale, M., Montomoli, F., D'Ammaro, A., Salvadori, S., Martelli, F., 2013. Uncertainty quantification: A stochastic method for heat transfer prediction using LES. Journal of Turbomachinery 135 (5), 051021.

[15] Chakravarthy, S., 1988. High resolution upwind formulations for the Navier-Stokes equations. In: Computational Fluid Dynamcis, VKI Lecture Series 1988-05, March 7–11.
[16] Commission, E., 2012. Flightpath 2050. Europe's vision for aviation. Report of the High Level Group on Aviation Research, Publications Office of the European Union, Luxembourg.
[17] Congedo, P. M., Duprat, C., Balarac, G., Corre, C., 2011. Effects of inlet uncertainties on prediction of turbulent flows using RANS and LES simulations. In: 20th AIAA Computational Fluid Dynamics Conference. p. 3869.
[18] Cressie, N., 1990. The origins of Kriging. Mathematical Geology 22 (3), 239–252.
[19] Datta, D., 2011. Non-probabilistic uncertainty analysis of analytical and numerical solution of heat conduction. International Journal of Energy, Information and Communications 2 (4), 143–156.
[20] De Baar, J., Scholcz, T. P., Verhoosel, C. V., Dwight, R. P., van Zuijlen, A. H., Bijl, H., 2012. Efficient uncertainty quantification with gradient-enhanced Kriging: Applications in fsi. ECCOMAS Vienna.
[21] Deb, K., Pratap, A., Agarwal, S., Meyarivan, T., 2002. A fast and elitist multiobjective genetic algorithm: NSGA-II. IEEE transactions on evolutionary computation 6 (2), 182–197.
[22] Dembowski, M. A., Georgiadis, N. J., 2002. An evaluation of parameters influencing jet mixing using the WIND Navier-Stokes code.
[23] Dessombz, O., Thouverez, F., Laîné, J.-P., Jézéquel, L., 2001. Analysis of mechanical systems using interval computations applied to finite element methods. Journal of Sound and Vibration 239 (5), 949–968.
[24] Dezitter, F., Bezard, H., de Saint Victor, X., Zeggai, K., Britchford, K., Joubert, G., Puigt, G., 2009. Installation effects characterization of VHBR engines part III: CFD assessment for jet mixing.
[25] Duchaine, F., Morel, T., M. Gicquel, L., 2009. Computational-fluid-dynamics-based kriging optimization tool for aeronautical combustion chambers. AIAA journal 47 (3), 631–645.
[26] Dwight, R. P., Han, Z.-H., 2009. Efficient uncertainty quantification using gradient-enhanced kriging. AIAA paper 2276, 2009.
[27] Eldred, M., Burkardt, J., 2009. Comparison of non-intrusive polynomial chaos and stochastic collocation methods for uncertainty quantification. AIAA paper 976 (2009), 1–20.
[28] Emami, B., Bussmann, M., Tran, H., 2010. Application of realizability and shock unsteadiness to k- ε simulations of under-expanded axisymmetric supersonic free jets. Journal of Fluids Engineering 132 (4), 041104.
[29] Erkoyuncu, J. A., 2011. Cost uncertainty management and modelling for industrial product-service systems. Ph.D. thesis, Cranfield University.
[30] Fang, H., Rais-Rohani, M., Liu, Z., Horstemeyer, M., 2005. A comparative study of metamodeling methods for multiobjective crashworthiness optimization. Computers & Structures 83 (25), 2121–2136.
[31] Fesanghary, M., Damangir, E., Soleimani, I., 2009. Design optimization of shell and tube heat exchangers using global sensitivity analysis and harmony search algorithm. Applied Thermal Engineering 29 (5), 1026–1031.
[32] Fiorentini, G., Lisi, E., Sarkar, S., Villante, F., 1998. Quantifying uncertainties in primordial nucleosynthesis without Monte Carlo simulations. Physical Review D 58 (6), 063506.
[33] Georgiadis, N. J., Yoder, D. A., Engblom, W. B., 2006. Evaluation of modified two-equation turbulence models for jet flow predictions. AIAA journal 44 (12), 3107–3114.
[34] Gorle, C., Emory, M., Iaccarino, G., 2011. Epistemic uncertainty quantification of RANS modeling for an under-expanded jet in a supersonic cross flow. CTR Annual Research Briefs, Center for Turbulence Research, Stanford University, Stanford, CA.
[35] Granados-Ortiz, F.-J., 2016. Uncertainty and sensitivity analysis of computational simulations of industrial jet flows. Ph.D. thesis, University of Greenwich, London.
[36] Granados-Ortiz, F.-J., Lai, C.-H., 2016. A novel framework for uncertainty propagation in multidisciplinary design life cycle for shock-cell noise research. In: 22nd CEAS/AIAA Aeroacoustics 2016, Lyon, France.
[37] Granados-Ortiz, F.-J., Ortega-Casanova, J., Lai, C.-H., 2015. Modelling for computational cost reduction and optimisation of an impinging swirling jet created by a rotating pipe with application to heat transfer from a heated solid flat plate. In: 8th International Congress on Industrial and Applied Mathematics. Beijing, (China). 10-14 August 2015.
[38] Halton, J. H., 1970. A retrospective and prospective survey of the Monte Carlo method. Siam review 12 (1), 1–63.
[39] Helton, J., Davis, F., 2003. Latin hypercube sampling and the propagation of uncertainty in analyses of complex systems. Reliability Engineering and System Safety 81, 23–69.
[40] Hiemstra, P. H., Pebesma, E. J., Twenhöfel, C. J., Heuvelink, G. B., 2008. Automatic real-time interpolation of radiation hazards: prototype and system architecture considerations. International Journal of Spatial Data Infras-

tructures Research 3, 58–72.

[41] Hosder, S., Maddalena, L., 2009. Non-intrusive polynomial chaos for the stochastic CFD study of a supersonic pressure probe. In: 47th AIAA Aerospace Sciences Meeting including The New Horizons Forum and Aerospace Exposition. p. 1129.

[42] Huang, P., Bardina, J., Coakley, T., 1997. Turbulence modeling validation, testing, and development. NASA Technical Memorandum 110446.

[43] Iaccarino, G., Mishra, A. A., Ghili, S., 2017. Eigenspace perturbations for uncertainty estimation of single-point turbulence closures. Physical Review Fluids 2 (2), 024605.

[44] Jansen, M. J., 1999. Analysis of variance designs for model output. Computer Physics Communications 117 (1), 35–43.

[45] Jouhaud, J.-C., Sagaut, P., Labeyrie, B., 2006. A kriging approach for CFD/wind-tunnel data comparison. Journal of Fluids Engineering 128 (4), 847–855.

[46] Kaushik, M., Kumar, R., Humrutha, G., 2015. Review of computational fluid dynamics studies on jets. American Journal of Fluid Dynamics 5 (A), 1–11.

[47] Kawai, S., Shimoyama, K., 2013. Kriging-model-based uncertainty quantification in computational fluid dynamics. In: 32nd AIAA Applied Aerodynamics Conference.

[48] Klimke, A., Willner, K., WOHLMUTH, B., 2004. Uncertainty modeling using fuzzy arithmetic based on sparse grids: applications to dynamic systems. International Journal of Uncertainty, Fuzziness and Knowledge-based Systems 12 (06), 745–759.

[49] Laurenceau, J., Meaux, M., 2008. Comparison of gradient and response surface based optimization frameworks using adjoint method. AIAA Paper 1889, 2008.

[50] Legleiter, C. J., Kyriakidis, P. C., 2008. Spatial prediction of river channel topography by kriging. Earth Surface Processes and Landforms 33 (6), 841–867.

[51] Lockwood, B. A., Rumpfkeil, M. P., Yamazaki, W., Mavriplis, D. J., 2011. Uncertainty quantification in viscous hypersonic flows using gradient information and surrogate modeling. AIAA Paper 885, 2011.

[52] Lophaven, S. N., Nielsen, H. B., Søndergaard, J., 2002. Dace: A MATLAB Kriging Toolbox. version 2.0. Tech. rep., DTU, tech. Report NASA/CR-2003-212153, NASA Langley Research Center.

[53] Lucor, D., Meyers, J., Sagaut, P., 2007. Sensitivity analysis of large-eddy simulations to subgrid-scale-model parametric uncertainty using polynomial chaos. Journal of Fluid Mechanics 585, 255–279.

[54] Mahaffy, J., Chung, B., Song, C., Dubois, F., Graffard, E., Ducros, F., Heitsch, M., Scheuerer, M., Henriksson, M., Komen, E., et al., 2007. Best practice guidelines for the use of CFD in nuclear reactor safety applications. Tech. rep., Organisation for Economic Co-Operation and Development.

[55] McDaniel, D., Cummings, R., Bergeron, K., Morton, S., Dean, J., 2007. Comparisons of CFD solutions of static and maneuvering fighter aircraft with flight test data. Tech. rep., DTIC Document.

[56] Metropolis, N., Ulam, S., 1949. The Monte Carlo method. Journal of the American statistical association 44 (247), 335–341.

[57] Mishra, A., Iaccarino, G., 2017. RANS predictions for high-speed flows using enveloping models. Center for Turbulence Research Annual Research Briefs 2016.

[58] Mishra, A., Iaccarino, G., Duraisamy, K., 2015. Epistemic uncertainty in statistical markovian turbulence models. CTR Annu. Res. Briefs 2015, 183–195.

[59] Mishra, A. A., Iaccarino, G., 2017. Uncertainty estimation for reynolds-averaged navier–stokes predictions of high-speed aircraft nozzle jets. AIAA Journal, 1–6.

[60] Mishra, A. A., Mukhopadhaya, J., Iaccarino, G., Alonso, J., 2018. An uncertainty estimation module for turbulence model predictions in su2. arXiv preprint arXiv:1803.00725.

[61] Montomoli, F., Carnevale, M., D'Ammaro, A., Massini, M., Salvadori, S., 2015. Uncertainty quantification in computational fluid dynamics and aircraft engines. Springer.

[62] Noorkami, M., Robinson, J. B., Meyer, Q., Obeisun, O. A., Fraga, E. S., Reisch, T., Shearing, P. R., Brett, D. J., 2014. Effect of temperature uncertainty on polymer electrolyte fuel cell performance. International Journal of Hydrogen Energy 39 (3), 1439–1448.

[63] Oberkampf, W. L., DeLand, S. M., Rutherford, B. M., Diegert, K. V., Alvin, K. F., 2002. Error and uncertainty in modeling and simulation. Reliability Engineering & System Safety 75 (3), 333–357.

[64] Onorato, G., Loeven, G., Ghorbaniasl, G., Bijl, H., Lacor, C., 2010. Comparison of intrusive and non-intrusive polynomial chaos methods for cfd applications in aeronautics. In: V European Conference on Computational

Fluid Dynamics ECCOMAS, Lisbon, Portugal. pp. 14–17.
[65] Ortega-Casanova, J., Granados-Ortiz, F., 2014. Numerical simulation of the heat transfer from a heated plate with surface variations to an impinging jet. International Journal of Heat and Mass Transfer 76, 128–143.
[66] Panda, J., 1998. Shock oscillation in underexpanded screeching jets. JFM 363, 173–198.
[67] Panda, J., 1999. An experimental investigation of screech noise generation. JFM 378, 71–96.
[68] Panda, J., Raman, G., Zaman, K., 2003. Underexpanded screeching jets from circular, rectangular, and elliptic nozzles. Tech. rep., NASA.
[69] Panizza, A., Bonini, A., Innocenti, L., 2015. Uncertainty quantification of hot gas ingestion for a gas turbine nozzle using polynomial chaos. In: ASME Turbo Expo 2015: Turbine Technical Conference and Exposition. American Society of Mechanical Engineers, pp. V02CT45A009–V02CT45A009.
[70] Payne, J. L., Roy, C. J., Beresh, S. J., 2001. A comparison of turbulence models for a supersonic jet in transonic cross flow. In: 39th AIAA Aerospace Science Meeting and Exhibit. pp. 2001–1048.
[71] Perez, R. A., 2008. Uncertainty analysis of computational fluid dynamics via polynomial chaos. Ph.D. thesis, Virginia Tech.
[72] Platteeuw, P., 2008. Application of the probabilistic collocation method to uncertainty in turbulence models. Ph.D. thesis, Delft University.
[73] Rao, S. S., Berke, L., 1997. Analysis of uncertain structural systems using interval analysis. AIAA journal 35 (4), 727–735.
[74] Rasmussen, C. E., 2004. Gaussian processes in machine learning. In: Advanced lectures on Machine Learning. Springer, pp. 63–71.
[75] Riley, M. E., Grandhi, R. V., 2011. Quantification of model-form and predictive uncertainty for multi-physics simulation. Computers & Structures 89 (11), 1206–1213.
[76] Roe, P. L., 1981. Approximate Riemann solvers, parameter vectors and difference schemes. Journal of Computational Physics 43 (2), 357–372.
[77] Saltelli, A., Ratto, M., Andres, T., Campolongo, F., Cariboni, J., Gatelli, D., Tarantola, S., 2008. Global sensitivity analysis: the primer. John Wiley & Sons.
[78] Schaefer, J., West, T., Hosder, S., Rumsey, C., Carlson, J.-R., Kleb, W., 2015. Uncertainty quantification of turbulence model closure coefficients for transonic wall-bounded flows. In: 22nd AIAA Computational Fluid Dynamics Conference. p. 2461.
[79] Seiner, J. M., Ponton, M. K., Jansen, B. J., Lagen, N. T., 1992. The effects of temperature on supersonic jet noise emission. In: 14th DGLR/AIAA aeroacoustics conference. Vol. 1. pp. 295–307.
[80] Shen, H., Tam, C. K., 1998. Numerical simulation of the generation of axisymmetric mode jet screech tones. AIAA Journal 36 (10), 1081–1807.
[81] Silva, R., Perez, M., Berenguel, M., Valenzuela, L., Zarza, E., 2014. Uncertainty and global sensitivity analysis in the design of parabolic-through direct steam generation plants for process heat applications. Applied Energy 121, 233–244.
[82] Simon, F., Guillen, P., Sagaut, P., Lucor, D., 2010. A gPC-based approach to uncertain transonic aerodynamics. Computer Methods in Applied Mechanics and Engineering 199 (17-20), 1091–1099.
[83] Simpson, T. W., Poplinski, J., Koch, P. N., Allen, J. K., 2001. Metamodels for computer-based engineering design: survey and recommendations. Engineering with computers 17 (2), 129–150.
[84] Sin, G., Gernaey, K. V., Neumann, M. B., van Loosdrecht, M. C. M., Gujer, W., 2011. Global sensitivity analysis in waste water treatment plant model applications: Prioritizing sources of uncertainty. Water Research 45 (2), 639–651.
[85] Sin, G., Lantz, A. E., Gernaey, K. V., 2009. Good modeling practice for pat applications: Propagation of input uncertainty and sensitivity analysis. Biotechnology progress. DOI 10.1021/bp.166.
[86] Smith, R. C., 2013. Uncertainty quantification: theory, implementation and applications. Vol. 12. SIAM.
[87] Smolyak, S., 1963. Quadrature and interpolation formulas for tensor products of certain classes of functions. Soviet Math. Dokl, 240–243.
[88] Song, W., Keane, A., Eres, H., Pound, G., Cox, S., 2003. Two dimensional airfoil optimisation using CFD in a grid computing environment. In: European Conference on Parallel Processing. Springer, pp. 525–532.
[89] Spalart, P., Allmaras, S., 1992. A one-equation turbulence model for aerodynamic flows. AIAA Paper 92-0439, 30th Aerospace Sciences Meeting and Exhibit, Reno, Nevada (1992).
[90] Spalart, P. R., Rumsey, C. L., 2007. Effective inflow conditions for turbulence models in aerodynamic calculations.

AIAA journal 45 (10), 2544–2553.

[91] Spanos, P. D., Ghanem, R., 1989. Stochastic finite element expansion for random media. Journal of engineering mechanics 115 (5), 1035–1053.

[92] Srivastava, V., Duraisamy, K., 2018. Aerodynamic design of aircraft engine nozzles with consideration of model form uncertainties. In: AIAA Non-Deterministic Approaches Conference. p. 2175.

[93] Tam, C. K., Burton, D. E., 1984. Sound generated by instability waves of supersonic flows. Part 2. Axisymmetric jets. Journal of Fluid Mechanics 138, 273–295.

[94] Taylor, S., Galea, E., Patel, M., Petridis, M., Knight, B., Ewer, J., 1997. SMARTFIRE: an integrated computational fluid dynamics code and expert system for fire field modelling. Fire Safety Science 5, 1285–1296.

[95] Tian, W., 2013. A review of sensitivity analysis methods in building energy analysis. Renewable Sustainable Energy Rev 20, 4–119.

[96] Tinoco, E. N., 2007. CFD uncertainty and validation for commercial aircraft applications. In: NATO Symposium AVT. Vol. 147.

[97] Van Gelder, L., Das, P., Janssen, H., Roels, S., 2014. Comparative study of metamodelling techniques in building energy simulation: Guidelines for practitioners. Simulation Modelling Practice and Theory 49, 245–257.

[98] van Leer, B., 1979. Towards the ultimate conservative difference scheme. V. A second-order sequel to Godunov's method. Journal of Computational Physics 32 (1), 101–136.

[99] Von Winckel, G., 2008. Fast clenshaw-curtis quadrature. Tech. rep., The Mathworks Central File Exchange, Mar. 2008. URL http://www.mathworks.com/matlabcentral/fileexchange/19063-sparse-grid-quadrature/content/spquad.m.

[100] Walters, R., Huyse, L., 2001. Stochastic methods for fluid mechanics-an introduction. Tech. rep., Tech. Rep. in preparation, ICASE, NASA Langley Research Center, Hampton, VA.

[101] Walz, N.-P., Hanss, M., 2013. Fuzzy arithmetical analysis of multibody systems with uncertainties. Archive of Mechanical Engineering 60 (1), 109–125.

[102] Warnes, J. J., 1986. A sensitivity analysis for universal Kriging. Mathematical Geology 18 (7), 653–676.

[103] Weber, C., 1998. Développement de méthodes implicites pour les équations de Navier-Stokes moyennes et la simulation des grandes échelles : Application à l'aérodynamique externe. Ph.D. thesis, Institut National Polytechnique de Toulouse, France.

[104] Wiener, N., 1938. The homogeneous chaos. American Journal of Mathematics 60 (4), 897–936.

[105] Witteveen, J. A., Doostan, A., Chantrasmi, T., Pecnik, R., Iaccarino, G., 2009. Comparison of stochastic collocation methods for uncertainty quantification of the transonic rae 2822 airfoil. In: Proceedings of workshop on quantification of CFD uncertainties.

[106] Witteveen, J. A., Iaccarino, G., 2013. Simplex stochastic collocation with ENO-type stencil selection for robust uncertainty quantification. Journal of Computational Physics 239, 1–21.

[107] Xiu, D., Karniadakis, G. E., 2003. Modeling uncertainty in flow simulations via generalized polynomial chaos. Journal of computational physics 187 (1), 137–167.

[108] Zadeh, L. A., 1968. Fuzzy algorithms. Information and control 12 (2), 94–102.